TECHNICAL UNIVERSITY OF CRETE

SCHOOL OF
ELECTRICAL AND COMPUTER ENGINEERING

DIPLOMA THESIS

Highway Traffic State Estimation and Control in Presence of Connected Automated Vehicles

Author

ALEXANDROS KONSTANTINOS VALTATZIS

Supervisor

Professor **MICHAIL G. LAGOUDAKIS**

Thesis Committee

Professor
MICHAIL G. LAGOUDAKIS
School of Electrical and Computer Engineering

Professor
MICHAIL ZERVAKIS
School of Electrical and Computer Engineering

Professor
IOANNIS PAPAMICHAIL
School of Production Engineering and Management

Chania, Crete 2023

Πολυτεχνείο Κρήτης

Σχολή
Ηλεκτρολόγων Μηχανικών και Μηχανικών Υπολογιστών

Διπλωματική Εργασία

Εκτίμηση Κατάστασης και Έλεγχος Κυκλοφορίας σε Αυτοκινητόδρομους Παρουσία Συνδεδεμένων Αυτόματων Οχημάτων

Συγγραφέας

Αλέξανδρος Κωνσταντίνος Βαλτατζής

Επιβλέπων

Καθηγητής Μιχαήλ Γ. Λαγουδάκης

Εξεταστική Επιτροπή

Καθηγητής
Μιχαήλ Γ. Λαγουδάκης
Σχολή Ηλεκτρολόγων Μηχανικών και Μηχανικών Υπολογιστών

Καθηγητής
Μιχαήλ Ζερβάκης
Σχολή Ηλεκτρολόγων Μηχανικών και Μηχανικών Υπολογιστών

Καθηγητής
Ιωάννης Παπαμιχαήλ
Σχολή Μηχανικών Παραγωγής και Διοίκησης

Χανιά, Κρήτη 2023

ABSTRACT

It is expected that the widespread adoption of Vehicle Automation and Communication Systems in the upcoming years will have a strong impact on freeway traffic performance. In addition to ensuring comfort and safety, other key objectives are to estimate and reduce traffic congestion, which constitute two related, substantial and demanding issues of the modern world. The aim of this diploma thesis is twofold. Its first objective is to demonstrate the efficiency of a macroscopic model-based approach, based on a Kalman filter, in estimating the total density and flow of vehicles in a real road network in Antwerp, Belgium, using real data and assuming that all vehicles are Connected Automated Vehicles (CAVs). The proposed filter utilizes only real speeds and a limited amount of real flow measurements from spot-sensors, on a 48Km motorway stretch that starts from A13 2100 in Boterlaar-Silsburg neighborhood and ends at A13 3945 in Ham municipality, Antwerp, Belgium. The accuracy and reliability of the estimated traffic states are assessed through comparison with ground truth measurements. The second goal of this diploma thesis is to show the effectiveness of utilizing an Adaptive Cruise Control (ACC) traffic control strategy in boosting the motorway traffic flow at active bottleneck locations by adjusting the time-gap of ACC-equipped vehicles in selected motorway sections in real-time, based on current and estimated traffic conditions. The proposed deployment and application scenario is implemented successfully in a toy road network in the Aimsun Next microsimulator, using the Gipps car-following model, which is known for its limitations in relation to the capacity drop phenomenon. The simulation results are displayed over different ACC penetration rates (the percentage of the CAVs present in the traffic) and prove that there is a significant improvement in the total time spent in the road network and in the average vehicle delay, as the penetration rate increases.

ΠΕΡΙΛΗΨΗ

Τα επόμενα χρόνια αναμένεται ότι η ευρεία υιοθέτηση των Συστημάτων Αυτοματισμού και Επικοινωνίας Οχημάτων (VACS) θα έχει σημαντικό αντίκτυπο στην απόδοση της κυκλοφορίας στους αυτοκινητόδρομους. Εκτός από τη διασφάλιση της άνεσης και της ασφάλειας, άλλοι βασικοί στόχοι είναι η εκτίμηση και η μείωση της κυκλοφοριακής συμφόρησης, που αποτελούν δύο σχετικά μεταξύ τους, ουσιαστικά και απαιτητικά ζητήματα του σύγχρονου κόσμου. Ο στόχος της παρούσας διπλωματικής εργασίας είναι διπλός. Ο πρώτος στόχος είναι να παρουσιάσει την αποτελεσματικότητα μιας μακροσκοπικής μοντελο-κεντρικής προσέγγισης, βασισμένης στη χρήση ενός φίλτρου Kalman, στην εκτίμηση της συνολικής πυκνότητας και ροής των οχημάτων σε ένα πραγματικό οδικό δίκτυο στην Αμβέρσα του Βελγίου, χρησιμοποιώντας πραγματικά δεδομένα και υποθέτοντας ότι όλα τα οχήματα είναι συνδεδεμένα αυτοματοποιημένα οχήματα (Connected Automated Vehicles - CAVs). Το προτεινόμενο φίλτρο χρησιμοποιεί μόνο μετρήσεις πραγματικής ταχύτητας και έναν περιορισμένο αριθμό μετρήσεων πραγματικής ροής οχημάτων από σημειακούς αισθητήρες, σε ένα τμήμα αυτοκινητόδρομου μήκους 48 χιλιομέτρων που ξεκινά από το A13 2100 στην περιοχή Boterlaar-Silsburg και τελειώνει στο A13 3945 στον Δήμο Ham, στην Αμβέρσα του Βελγίου. Η ακρίβεια και η αξιοπιστία των εκτιμώμενων καταστάσεων κυκλοφορίας αξιολογούνται μέσω σύγκρισης με πραγματικές μετρήσεις. Ο δεύτερος στόχος της παρούσας διπλωματικής εργασίας είναι να αναδείξει την αποτελεσματικότητα της χρήσης μιας στρατηγικής ελέγχου κυκλοφορίας, βασισμένης σε Adaptive Cruise Control (ACC), για την ενίσχυση της κυκλοφοριακής ροής σε ενεργές θέσεις συμφόρησης (bottlenecks) αυτοκινητόδρομων, προσαρμόζοντας το χρονικό διάστημα (time-gap) των οχημάτων εξοπλισμένων με ACC σε επιλεγμένα τμήματα αυτοκινητόδρομων σε πραγματικό χρόνο, με βάση τις τρέχουσες και τις εκτιμώμενες συνθήκες κυκλοφορίας. Το προτεινόμενο σενάριο ανάπτυξης και εφαρμογής υλοποιείται με επιτυχία σε ένα τεχνητό οδικό δίκτυο στον μικροπροσομοιωτή Aimsun Next, χρησιμοποιώντας με επιτυχία το μοντέλο Gipps car-following, το οποίο είναι γνωστό για τους περιορισμούς του όσον αφορά στο φαινόμενο μείωσης χωρητικότητας (capacity drop). Τα αποτελέσματα της προσομοίωσης παρουσιάζονται για διαφορετικά ποσοστά διείσδυσης ACC (δηλαδή, το ποσοστό των οχημάτων CAVs που υπάρχουν στην κυκλοφορία, γνωστό ως penetration rate) και αποδεικνύουν ότι υπάρχει σημαντική βελτίωση στον συνολικό χρόνο που δαπανάται από όλα τα οχήματα στο οδικό δίκτυο και στη μέση καθυστέρηση καθενός οχήματος, καθώς αυξάνεται το ποσοστό διείσδυσης των ACC οχημάτων.

ACKNOWLEDGEMENTS

This thesis, as well as my studies, would not have been possible without the constant support of my family. I am forever grateful to my mother, my father, my sister and all those in my family who supported me all these years of my life and taught me to stand up for myself, claim my rights and fight for the good of the people. I am extremely thankful to Vasileios Markantonakis, PhD student and research associate at the Dynamic Systems & Simulation Laboratory (DSSL), for supporting me with his guidance, knowledge, availability and patience throughout my thesis. I would also like to express my gratitude to Professor Ioannis Papamichail for his time, key advices and supervision. Last, but not least, I would like to thank Professor Michail G. Lagoudakis for finding the time for me, when there was not much time for himself, for listening to me and for helping me with great interest in finding a topic for my thesis. This thesis has been conducted partially in the framework of the project FRONTIER, which has received funding from the European Commission under Grant Agreement No: 955317.

FRONTIER
FUTURE MOBILITY

TABLE OF CONTENTS

ABSTRACT 1

ΠΕΡΙΛΗΨΗ 3

ACKNOWLEDGEMENTS 5

1 INTRODUCTION 15
- 1.1 SETTING THE STAGE . . . 15
- 1.2 A PREVIEW OF CHAPTER 2 . . . 16
- 1.3 A PREVIEW OF CHAPTER 3 . . . 17
- 1.4 THESIS CONTRIBUTION AND PROPOSED RECOMMENDATIONS 18

2 HIGHWAY TRAFFIC STATE ESTIMATION 19
- 2.1 THE DYNAMICS OF TRAFFIC DENSITY AS A LPV SYSTEM . . . 19
  - 2.1.1 FULL RAMP-FLOW AVAILABILITY . . . 20
  - 2.1.2 PARTIAL RAMP-FLOW AVAILABILITY . . . 21
- 2.2 KALMAN FILTER . . . 23
- 2.3 NETWORK DESCRIPTION . . . 23
- 2.4 TRAFFIC DATA COLLECTION ALGORITHM . . . 25
- 2.5 PARAMETER TUNING . . . 28
- 2.6 ESTIMATION RESULTS . . . 29

3 HIGHWAY TRAFFIC CONTROL WITH ACC-VEHICLES 39
- 3.1 THE AIMSUN NEXT MICROSCOPIC SIMULATOR . . . 39
- 3.2 BEHAVIORAL MODELS . . . 39
  - 3.2.1 CAR-FOLLOWING MODEL . . . 40
    - MODIFIED MODEL FOR CONGESTED HIGHWAYS . . . 42
    - ADAPTIVE CRUISE CONTROL (ACC) CAR-FOLLOWING 43
  - 3.2.2 LANE-CHANGING MODEL . . . 44
    - GIPPS LANE-CHANGING MODEL . . . 45
    - HEURISTIC RULES ON LANE-CHANGING MODEL . . . 46
- 3.3 REAL-TIME ACC-BASED TRAFFIC CONTROL ADAPTATION STRATEGY . . . 47
  - 3.3.1 CAPACITY INCREASE . . . 48
  - 3.3.2 DISCHARGE FLOW INCREASE . . . 49
- 3.4 NETWORK . . . 49
- 3.5 SIMULATION PARAMETER SETUP . . . 50

3.6 EXPERIMENTAL RESULTS 53
3.6.1 NO ACC CONTROL ADAPTATION 53
3.6.2 ACC CONTROL ADAPTATION SCENARIO 1 57
3.6.3 ACC CONTROL ADAPTATION SCENARIO 2 60
3.6.4 NO ACC CONTROL ADAPTATION AND ACC CONTROL ADAPTATION SCENARIOS 1 AND 2 64

4 CONCLUSIONS AND FUTURE WORK **69**
4.1 CONCLUSIONS 69
4.2 FUTURE WORK 70

BIBLIOGRAPHY **71**

LIST OF FIGURES

2.1 Network position in Belgium 24
2.2 Selected network stretch 24
2.3 Setup diagram 25
2.4 CV_ρ considering various powers of the σ_Q filter parameter . . 29
2.5 CV_ρ considering various powers of the $\sigma_{Q_{Un}}$ filter parameter . 30
2.6 CV_ρ considering various powers of the σ_R filter parameter . . 31
2.7 Average weighted speeds of real sensor groups 12-13 in km/h on 22/9/2022 32
2.8 Average weighted speeds of real sensor groups 14-15 in km/h on 22/9/2022 32
2.9 Average weighted speeds of real sensor groups 16-17 in km/h on 22/9/2022 32
2.10 Total flows of real sensor groups 12-13 in veh/h on 22/9/2022 33
2.11 Total flows of real sensor groups 14-15 in veh/h on 22/9/2022 33
2.12 Total flows of real sensor groups 16-17 in veh/h on 22/9/2022 33
2.13 Flow, Density, Fundamental Diagram and Speed of segment 24 on 22/9/2022 34
2.14 Comparison between ground truth (blue line) and estimated (black line) traffic density at segments 9 and 15 for 22/09/2022 34
2.15 Comparison between ground truth (blue line) and estimated (black line) traffic density at segments 24 and 31 for 22/09/2022 35
2.16 Comparison between ground truth (blue line) and estimated (black line) traffic density at segments 24 and 31 for 04/01/2023 35
2.17 Comparison between ground truth (blue line) and estimated (black line) traffic density at segment 24 for 05/01/2023 (left) and at segment 62 for 06/01/2023 (right) 36
2.18 Comparison between real (left) and estimated (right) density for Thursday 22/09/2022 36
2.19 Comparison between real (left) and estimated (right) density for Wednesday 04/01/2023 37
2.20 Comparison between real (left) and estimated (right) density for Thursday 05/01/2023 37
2.21 Comparison between real (left) and estimated (right) density for Friday 06/01/2023 38

3.1 Sensitivity factor types and their impact 42

3.2 Heuristics replacing the default lane-changing model 47
3.3 Illustration of the control strategy in action 48
3.4 Time-gap strategy using: (a) a linear, or (b) a stepwise function [5] 48
3.5 The toy network developed in the Aimsun Next tool for testing the two ACC control adaptation scenarios 50
3.6 Speed contour plot of the toy network 51
3.7 Traffic flow, density, fundamental diagram and speed of section 8 51
3.8 Heuristic lane-changing rules applied in the acceleration lane of section 8 in the toy network 52
3.9 Heuristic lane-changing rules applied in the middle lane of section 8 in the toy network 53
3.10 No ACC Control Adaptation case for PR 0%, 50% and 100% . 54
3.11 No ACC Control Adaptation case: Total Time Spent (TTS) considering various PR 55
3.12 No ACC Control Adaptation case: Average Vehicle Delay (AVD) considering various PR 55
3.13 ACC Control Adaptation scenario 1 for PR 20%, 50% and 100% 57
3.14 ACC Control Adaptation scenario 1: Total Time Spent (TTS) considering various PR 58
3.15 ACC Control Adaptation scenario 1: Average Vehicle Delay (AVD) considering various PR 58
3.16 ACC Control Adaptation scenario 1: Flow, density, ACC time-gap suggestions made by the strategy and speed at section 8 for PR=30% 59
3.17 ACC Control Adaptation scenario 2 for PR 20%, 50% and 100% 60
3.18 ACC Control Adaptation scenario 2: Total Time Spent (TTS) considering various PR 61
3.19 ACC Control Adaptation scenario 2: Average Vehicle Delay (AVD) considering various PR 61
3.20 ACC Control Adaptation scenario 2: Flow, density, ACC time-gap suggestions made by the strategy and speed at section 8 for PR=30% 62
3.21 ACC Control Adaptation scenario 2: Flow, density, ACC time-gap suggestions made by the strategy and speed at section 9 for PR=30% 63
3.22 Comparison of the Total Time Spent (TTS) for the No ACC Control Adaptation case, the ACC Control Adaptation scenarios 1 and 2 considering various PR 64
3.23 Comparison of the Average Vehicle Delay (AVD) for the No ACC Control Adaptation case, the ACC Control Adaptation scenarios 1 and 2 considering various PR 65
3.24 Subtraction of the Total Time Spent (TTS) between the No ACC Control Adaptation case, the ACC Control Adaptation scenarios 1 and 2 considering various PR 66

3.25 Subtraction of the Average Vehicle Delay (AVD) between the No ACC Control Adaptation case, the ACC Control Adaptation scenarios 1 and 2 considering various PR 67

LIST OF TABLES

2.1 Segment characteristics 26
2.2 Class number per vehicle length and type 27

3.1 No ACC Control Adaptation case: Total Time Spent (TTS) and Average Vehicle Delay (AVD) considering various PR 54
3.2 ACC Control Adaptation scenario 1: Total Time Spent (TTS) and Average Vehicle Delay (AVD) considering various PR . . 57
3.3 ACC Control Adaptation scenario 2: Total Time Spent (TTS) and Average Vehicle Delay (AVD) considering various PR . . 60
3.4 Difference between ACC Control Adaptation scenario 1 and 2 in Total Time Spent (TTS) and Average Vehicle Delay (AVD) metrics considering various PR 66

CHAPTER 1

INTRODUCTION

1.1 SETTING THE STAGE

Traffic congestion is a significant and widely recognized issue in major cities of the modern world. Each day, the volume of vehicles concentrated on urban roads continues to rise in a way that the road infrastructure cannot efficiently cope with, especially during peak hours. Consequently, speeds decrease, travel times lengthen, and vehicles accumulate in lengthy queues. As a result, people experience delays in reaching personal and professional appointments, while vehicles providing vital medical services struggle to make it in time. Furthermore, the frequency of road accidents increases and the emission of exhaust gases notably rises as a direct consequence.

Vehicle Automation and Communication Systems (VACS) can play a determinant role in greatly reducing accidents on the road, emissions and, notably, alleviate traffic congestion, reshaping the future of transportation. These advanced systems integrate a variety of technology to improve driving comfort, efficiency, and safety. VACS enable vehicles to communicate with each other (V2V) and with infrastructure (V2I), facilitating better traffic management, congestion reduction, and optimized routing.

Due to the challenges involved in expanding road networks, improving the efficiency of existing traffic systems requires considerable effort. Therefore, traffic management utilizing VACS emerges as a viable solution to enhance performance without significant infrastructure changes. For this reason, both traffic authorities and automobile industries are presently emphasizing on the development of innovative techniques in traffic monitoring [1]. Traffic monitoring with the use of VACS can also facilitate traffic control strategies, with the use of VACS as well.

Generally, traffic monitoring is achieved with methods like measuring traffic flow with a sufficient amount of sensors to secure traffic monitoring accuracy, using surveillance cameras and GPS or satellite tracking. This helps traffic authorities make decisions aiming to improve traffic conditions, when this is needed. But, implementing such methods in a large scale would require a lot of hardware and, consequently, high installation and maintenance costs and environmental damage.

Traffic estimation with the use of VACS can be a low-cost solution to this problem. Connected vehicles can report, in real-time, to local or central authorities various types of traffic data, like their speed, or their urgency to reach a specific destination and get a real-time response [2]. These authorities can use this data and try to apply one or more traffic control strategies, according to the situation. These strategies would aim to optimize route planning based on the urgency of the trip, or based on minimizing CO_2, or they would target the maximum reduction of congestions. Connected automated vehicles (CAVs) can, not only play a very important role in materializing traffic estimation, but also, receive a control suggestion or command to implement a specific driving behaviour, according to the conditions, and therefore, avoid the formation of a congestion.

But, in order for CAVs to play these roles, the appropriate infrastructure is necessary. Although fully automated highways are unlikely to emerge very soon, partially automated highways already exist [1]. An essential part of such automated systems is the Adaptive Cruise Control (ACC), which is already implemented by many automotive manufacturers and it is in use.

The ACC system aims at increasing comfort and safety [3], but can, also, determinedly contribute to the aforementioned goals. Depending on the penetration rate of the ACC-vehicles on the road, that is, the percentage of ACC-vehicles in the total vehicle population, traffic estimation's precision and traffic control's influence on the traffic conditions can be evaluated accordingly. The higher the ACC penetration rate, the more accurate the estimation of traffic (see [1]), and the more effective the traffic control. The first one is due to the percentage of vehicles that are able to report their speed, and the second one is due to the percentage of vehicles that are able to implement one or more control strategies suggested or imposed by a local or central authority, as the ACC feature influences the traffic flow attributes.

1.2 A PREVIEW OF CHAPTER 2

The second chapter (HIGHWAY TRAFFIC STATE ESTIMATION) presents an algorithm that consists of real-time collecting, cleaning and processing real data from a selected highway stretch starting from A13 2100 in Boterlaar - Silsburg neighbourhood and ending at A13 3945 in Ham municipality, Antwerp, Belgium, and then passing them to a Kalman filter, developed in [4] and [1], in order to estimate traffic density.

The network in Antwerp uses several densely placed per-lane spot-sensors for measuring traffic flow and traffic speed. So, at intervals of some hundred or thousand meters, an amount of spot-sensors equal to the number of lanes exist.

Regarding the filter, it outputs estimated traffic density values for each and every road section at every estimation interval. For this, a limited, but sufficient to guarantee observability, amount of spot-detectors measure traffic flow, whilst the connected automated vehicles (CAVs) communicate their speed to a road-side unit (RSU) via V2I communication. But, since the data come from a real network in which the speeds of the vehicles are measured only by spot-sensors and not transmitted via V2I communication, the ACC penetration rate is assumed 100%.

The structure of this chapter is as follows. First, the traffic density of a motorway stretch subdivided into sections (or, equivalently, segments) is analyzed as a linear parameter-varying (LPV) system with the cases being two: *i*) all ramp traffic flow measurements are available and *ii*) not all ramp traffic flow measurements are available. Then, the Kalman filter used is exhibited and the network in Antwerp with its characteristics is displayed. After this, the traffic data collection algorithm that collects, cleans and processes the network's data follows. At the end, the system parameters that need tuning are examined and then are chosen. Finally, the estimation results are compared to the ground truth to illustrate the effectiveness of the filter on different traffic conditions (free-flow and congestion). So, the unused measurements are employed as the ground truth for comparison with the estimation results.

1.3 A PREVIEW OF CHAPTER 3

The third chapter (HIGHWAY TRAFFIC CONTROL WITH ACC-VEHICLES) presents a real-time, ACC-based traffic control adaptation strategy, developed in [5], aiming to delay, reduce and, if possible, annihilate traffic congestion in active bottleneck locations, with the successful use of the Gipps car-following model. In a real network, this can be achieved by measuring traffic flow via spot-detectors and vehicle speed via V2I communication from the CAVs in a section to a local RSU, or with spot-sensors. Then, the RSU imposes a time-gap, that is, the time-distance between two successive vehicles as they move along a roadway, to the ACC-vehicles based on the traffic flow and speed conditions in each section.

The control strategy consists of two distinct actions: *i*) gradual reduction of ACC time-gaps during near-capacity traffic to increase capacity and application of maximum time-gaps to ACC-vehicles, if congestion still manages to form and *ii*) on top of the first action, minimum time gaps are applied near active bottleneck locations to increase discharge flow. The scenario developed is simulated in the Aimsun Next microsimulator on a toy network.

The structure of this chapter is as follows. Initially, the Aimsun Next microsimulator is presented. Then, Aimsun Next's default behavioral models are presented with the car-following model (Gipps) being analyzed, highlighting its limitations in relation to the capacity drop phenomenon, and then the lane-changing model (Gipps) is getting replaced by heuristic rules at the bottleneck's section, as the default model also has limitations in merging areas. Afterwards, the real-time ACC-based traffic control adaptation strategy is examined by explaining the two aforementioned ACC-based time-gap actions: capacity increase and discharge flow increase. Subsequently, the considered toy network is depicted with all parameters that are critical in creating a congestion with the employed traffic models and with the display of the initial 100%-conventional-vehicles case, highlighting the congestion that has been created. Last, but not least, the experimental results are demonstrated for different penetration rates, proving that the first control action makes a significant impact in reducing the congestion from even small penetration rates, while the second one (on top of the first) practically surpasses the first at all times for all ACC penetration rates, ending up annihilating the congestion.

1.4 THESIS CONTRIBUTION AND PROPOSED RECOMMENDATIONS

The current diploma thesis was conducted at the Dynamic Systems & Simulation Laboratory (DSSL).

As for the second chapter (HIGHWAY TRAFFIC STATE ESTIMATION), an easy-to-use traffic data collection algorithm has been developed in order for real data to be collected and processed in real-time from any real existing traffic network. Then, this algorithm is used for collecting and processing the data by-the-day from a network in Antwerp and passing them to an already developed Kalman filter, which is used as a tool for traffic density estimation, and whose parameters are tuned anew, accordingly with the new data. Each day sampled is assessed with the criterion being if there had been congestion or not, in order to show it in this thesis.

Regarding the third chapter (HIGHWAY TRAFFIC CONTROL WITH ACC-VEHICLES), the simulation scenario of a toy network, for various ACC-vehicle penetration rates, with DSSL's ACC-controller, is carried out with the use of a different car-following model, the Gipps car-following model, for the first time. The Gipps model is known for its ability to account for the intricate dynamics of car-following, such as acceleration, deceleration, and the consideration of safety gaps between vehicles, but it does not sufficiently represent the behavior of drivers at very low speeds or during traffic congestion, where drivers may follow different driving strategies to maneuver through the traffic. So, the calibration process of the car-following and the lane-changing models, and of the ACC-controller on the selected network, has been conducted in the context of this thesis. Then, the network simulation aims to explore the integration of ACC-vehicles with and without the ACC-controller into the existing traffic flow, with the target being the traffic congestion's mitigation. What has been discovered is that with the appropriate Sensitivity Factor per segment, the Gipps car-following model is able create a relatively strong congestion.

Finally, in the end, it is suggested that the presented traffic estimation and traffic control techniques should be employed together, for maximizing driving efficiency, safety, comfort and ecological benefits, and minimizing the time spent in vehicular queues and traffic jams.

CHAPTER 2

HIGHWAY TRAFFIC STATE ESTIMATION

2.1 THE DYNAMICS OF TRAFFIC DENSITY AS A LPV SYSTEM

Consider a motorway stretch divided into segments of 0.4km - 0.7km each. The density $\rho_i(k)$ of segment i at time step k is defined as the number of vehicles in this segment by its length Δ_i. The traffic dynamics for the density can be described by the following discrete-time equations:

$$\rho_i(k+1) = \rho_i(k) + \frac{T}{\Delta_i}(q_{i-1}(k) - q_i(k) + r_i(k) - s_i(k)) \tag{2.1}$$

where $i \in [1, N]$ with N being the total number of segments of the motorway, k is the discrete time index, T is the discretization timestep, Δ_i is measured in km, q_i is the flow (veh/h) at the end of segment i and r_i and s_i are the inflow and outflow (veh/h) from an on-ramp or an off-ramp of segment i, respectively. Typically, a segment can include at most one ramp, either an on-ramp or an off-ramp. Empirically, a segment's length must be at most 700m in order for the estimation results to be accurate.
Using the known relation:

$$q_i = \rho_i v_i \tag{2.2}$$

where v_i is the arithmetic mean vehicle speed (km/h) in segment i, 2.1 becomes:

$$\rho_i(k+1) = \tfrac{T}{\Delta_i} v_{i-1}(k)\rho_{i-1}(k) + \left(1 - \tfrac{T}{\Delta_i} v_i(k)\right)\rho_i(k) + \tfrac{T}{\Delta_i}\left(r_i(k) - s_i(k)\right) \tag{2.3}$$

In order for the discrete-time relations 2.2, 2.3 to be sufficiently accurate, the inequality:

$$\max_{i,k} \frac{T}{\Delta_i} v_i(k) < 1 \tag{2.4}$$

must hold.

2.1.1 FULL RAMP-FLOW AVAILABILITY

In this subsection, we assume that all ramps contain a functional flow spot-detector that measures their flow. This theory is developed in [4].

Assuming that the average speed of conventional vehicles is roughly equal to the average speed of connected vehicles (which are reporting to the traffic authority), one can deduce that the segment speeds v_i are measured [4]. Therefore, the state-vector is

$$x = (\rho_1, ..., \rho_N)^T \tag{2.5}$$

and 2.3 can be written in the form of a LPV system:

$$x(k+1) = A(v(k))x(k) + Bu(k) \tag{2.6}$$

$$y(k) = Cx(k) \tag{2.7}$$

where

$$A(v(k)) = \begin{cases} a_{ij} = \frac{T}{\Delta_i} v_{i-1}(k), & if\ i-j = 1\ and\ i \geq 2 \\ a_{ij} = 1 - \frac{T}{\Delta_i} v_i(k), & if\ i = j \\ a_{ij} = 0, & otherwise \end{cases} \tag{2.8}$$

$$B = \begin{cases} b_{ij} = \frac{T}{\Delta_i}, & if\ i = 1\ and\ j = \{1,2\}\ or\ j-i = 1\ and\ i\ \geq 2 \\ b_{ij} = 0, & otherwise \end{cases} \tag{2.9}$$

$$u(k) = \begin{bmatrix} q_0(k) & r_1(k) - s_1(k) & ... & r_N(k) - s_N(k) \end{bmatrix}^T \tag{2.10}$$

$$C = \begin{bmatrix} 0 & ... & 0 & 1 \end{bmatrix} \tag{2.11}$$

with $v = [v_1\ ...\ v_N]^T \in \mathbb{R}^N$, $A \in \mathbb{R}^{N \times N}$, $B \in \mathbb{R}^{N \times (N+1)}$, $C \in \mathbb{R}^{1 \times N}$, where q_0 is the inflow of vehicles in the first segment, i.e. the entry of the selected motorway. q_0 along with r_i and s_i are inputs to system 2.6, while v_i are viewed as time-varying parameters of 2.6. Note that linear parameter-varying (LPV) systems are linear state-space models, whose traffic dynamics vary as a function of certain time-varying parameters. LPV systems are a subclass of linear time-varying (LTV) systems.

As output y of the system, the state variable ρ_N at the exiting segment N can be obtained via $\rho_N = \frac{q_N}{v_N}$ using flow measurements in segment N. In other words, a fixed flow detector must be stationed in the last segment. This is a necessary requirement for the system defined by 2.6-2.11 to be observable, as proven in [4] where this model is defined.

Last, but not least, as a means to the input u and the output y to be measured, it is required that the vehicle flows q_0 and q_N be measured via conventional detectors in the first and the last segment, respectively. So, conventional flow detectors are needed at the first and the last segment and at every ramp.

2.1.2 PARTIAL RAMP-FLOW AVAILABILITY

It is normal for a detector to start malfunctioning at some point of its life, as it happens with all electronics, mostly due to power cuts, weather or time. In this estimation scheme, this creates a problem in measuring the input flows r_i, s_i of the model in equation 2.10. So, instead of measuring r_i and s_i, the mainstream flow of the next segment can be directly measured. For instance, let us consider a segment i containing an off-ramp or an on-ramp with faulty or continuously no measurements. This means that some vehicles have left the stream and the estimator keeps counting them in (off-ramp case) or some vehicles have inserted the stream and the estimator does not include them in its computations (on-ramp case). The solution is simple; the flow of segment $i-1$ is known, so by just measuring the flow of $i+1$ one can determine the flow of segment i. This changes the state-space described in 2.5-2.11. The following theory is developed in [1].

Now, the flows of the unmeasured ramps should be added to the state-space. But first, some definitions should precede.

The scalar numbers l_r and l_s are the numbers of on-ramp and off-ramp flows, respectively, which are not being directly measured. Hence, the sets $L_r = \{n_1, ..., n_{l_r}\}$ and $L_s = \{n_{l_r+1}, ..., n_{l_r+l_s}\}$ are the sets of segments, denoted by n_i, which contain an on-ramp or an off-ramp, respectively, whose flows are not measured.

As it is common practice in estimation applications while addressing unknown quantities, we assume that any unmeasured on-ramp and off-ramp flows are constant, or, effectively, slowly varying, so that the unmeasured ramp flow dynamics may be reflected by a random walk [1]. The random walk equation follows:

$$\theta_i(k+1) = \theta_i(k) + \xi_i^{\theta}(k) \tag{2.12}$$

where ξ_i^{θ} is zero-mean white Gaussian noise and

$$\theta_i = \begin{cases} \frac{T}{\Delta_i} r_{n_i} & if\ n_i \in L_r \\ \frac{T}{\Delta_i} s_{n_i} & if\ n_i \in L_s \end{cases} \tag{2.13}$$

for all $i = 1, ..., l_r + l_s$.

Consequently, the state-vector of 2.5 becomes:

$$x = \left(\rho_1, ..., \rho_N, \theta_1, ..., \theta_{l_r+l_s}\right)^T, \tag{2.14}$$

since the segment speeds v_i, $i = 1, ..., N$ are reported by connected vehicles as stated above (2.5).

Before analysing the new, more generic system, some additional definitions ought to be listed:
$\bar{L} = L_r \cup L_s$ is the set of segments, which contain a ramp whose flow is not measured. $\bar{L}^* = \{n_1^*, n_2^*, ..., n_{l_r+l_s}^*\}$ is the set $\bar{L}$ ordered by $<$. $N_1 = N + l_r + l_s$ is the size of the set, which contains all the segments and the unmeasured ramps, while $N_2 = N - l_r - l_s$ is the size of the set of segments, which contain a ramp whose flow is directly measured, or no ramp at all. So, since

2.6 and 2.7 hold, then the new matrices are $A \in \mathbb{R}^{N_1 \times N_1}$, $B \in \mathbb{R}^{N_1 \times (N_2+1)}$ and $C \in \mathbb{R}^{(l_r+l_s)\times(N+l_r+l_s)}$. Additionally, the segment where the i-th measured ramp is positioned is denoted by m_i. So, the entries of matrix B that correspond to a measured ramp are set equal to $\frac{T}{\Delta_{m_i}}$, if $j = i+1$.

The deterministic part of the dynamics of segment densities given in 2.3 and of θ_i given in 2.12 can be written in the form of a LPV system. So, the matrices A, B, C and the input u of 2.6 and 2.7 change from 2.8-2.11 to 2.15-2.18:

$$A(v(k)) = \begin{cases} a_{ij} = \frac{T}{\Delta_i} v_{i-1}(k), & \textit{if } i - j = 1 \textit{ and } i \geq 2 \\ a_{ij} = 1 - \frac{T}{\Delta_i} v_i(k), & \textit{if } i = j \\ a_{n_i j} = 1, & \textit{if } n_i \in L_r \textit{ and } j = N + i \\ a_{n_i j} = -1, & \textit{if} n_i \in L_s \textit{ and } j = N + i \\ a_{ij} = 1, & \textit{if } N < i \leq N_1 \textit{ and } j = i \\ a_{ij} = 0, & \textit{otherwise} \end{cases} \tag{2.15}$$

$$B = \begin{cases} b_{ij} = \frac{T}{\Delta_i}, & \textit{if } i = 1 \textit{ and } j = 1 \\ b_{m_i j} = \frac{T}{\Delta_{m_i}}, & \textit{if } m_i \notin \bar{L},\ 1 \leq m_i \leq N, \\ & 1 \leq i \leq N_2 \textit{ and } j = i + 1 \\ b_{ij} = 0, & \textit{otherwise} \end{cases} \tag{2.16}$$

$$u(k) = \begin{cases} u_i = q_0(k), & \textit{if } i = 1 \\ u_{i+1} = r_{m_i} - s_{m_i}, & \textit{if } m_i \notin \bar{L} \end{cases} \tag{2.17}$$

$$C = \begin{cases} c_{ij} = 1, & \textit{for all } i = \{1, ..., l_r + l_s - 1\} \\ & \textit{and some } n_i^* \leq j \leq n_{i+1}^* - 1 \\ c_{ij} = 1, & \textit{if } i = l_r + l_s \textit{ and } j = N \\ c_{ij} = 0, & \textit{otherwise} \end{cases} \tag{2.18}$$

To illustrate the practical meaning of the input u, one can see from 2.17 that the flow of vehicles q_0 at the entry of the selected stretch, together with any measured on-ramp flows r_i, $i \notin L_r$ and off-ramp flows s_i, $i \notin L_s$ are measured inputs to system 2.6.

As mentioned before, one of the measured outputs is the flow q_N at the mainstream exit of the stretch. This can be seen at the second value assignment of 2.18. q_N is available by a fixed flow detector, and so the last segment's density is obtained by $\rho_N = \frac{q_N}{v_N}$, where v_N is reported by connected vehicles.

The other outputs that may need to be measured by flow detectors are some mainstream measurements. More specifically, in the case of exactly one unmeasured ramp within the selected motorway stretch, no additional measurements are needed for flow observability. On the contrary, if there are two consecutive unmeasured ramps anywhere within the selected stretch, then one (any) mainstream flow measurement between these two ramps is needed for flow observability.

Summarizing, in order for the estimation algorithm to work, it is required that the measured - by fixed detectors - inputs are the mainstream total flow q_0 at the entry of the selected motorway stretch and any directly measured ramp flows r_i, $i \notin L_r$, s_i, $i \notin L_s$, and that the measured - by fixed detectors - outputs are the mainstream flow q_N of the last segment N and any mainstream flow q_i of segment i between two consecutive unmeasured ramps. Also, it is reminded that the average speed of all vehicles at a segment is roughly equal to the average speed reported by connected vehicles in the same segment via frequent messaging.

2.2 KALMAN FILTER

We utilize a Kalman filter [1] in order to estimate the traffic state of the network. Defining:

$$\hat{x} = \left(\hat{\rho}_1, ..., \hat{\rho}_N, \hat{\theta}_1, ..., \hat{\theta}_{l_r+l_s}\right)^T, \tag{2.19}$$

as the system state estimate, the filter equations are:

$$\hat{x}(k+1) = A(v(k))\hat{x}(k) + Bu(k) + A(v(k))K(k)(z(k) - C\hat{x}(k)) \tag{2.20}$$

$$K(k) = P(k)C^T(CP(k)C^T + R)^{-1} \tag{2.21}$$

$$P(k+1) = A(v(k))(I - K(k)C)P(k)A(v(k))^T + Q, \tag{2.22}$$

where the measurement z is a noisy version of y, and $Q = Q^T > 0$, $R = R^T > 0$ are tuning parameters which are discussed further later. In the ideal case in which there is additive, zero-mean Gaussian white noise in the state and output equations, Q and R represent the covariance matrices of the process and measurement noise, respectively. The initial conditions of the filter described by 2.20-2.22 are:

$$\hat{x}(k_0) = \mu \tag{2.23}$$

$$P(k_0) = H, \tag{2.24}$$

where μ and $H = H^T > 0$, in the ideal case, in which $x(k_0)$ is a Gaussian random variable, represent the mean and auto covariance matrix of $x(k_0)$, respectively.

2.3 NETWORK DESCRIPTION

The infrastructure network to be used in this thesis, is a motorway stretch in Antwerp, Belgium. The selected stretch starts at A13 2100 in Boterlaar - Silsburg neighbourhood and ends at A13 3945 in Ham municipality. The network as seen from Google Earth Pro is shown in Figure 2.1.

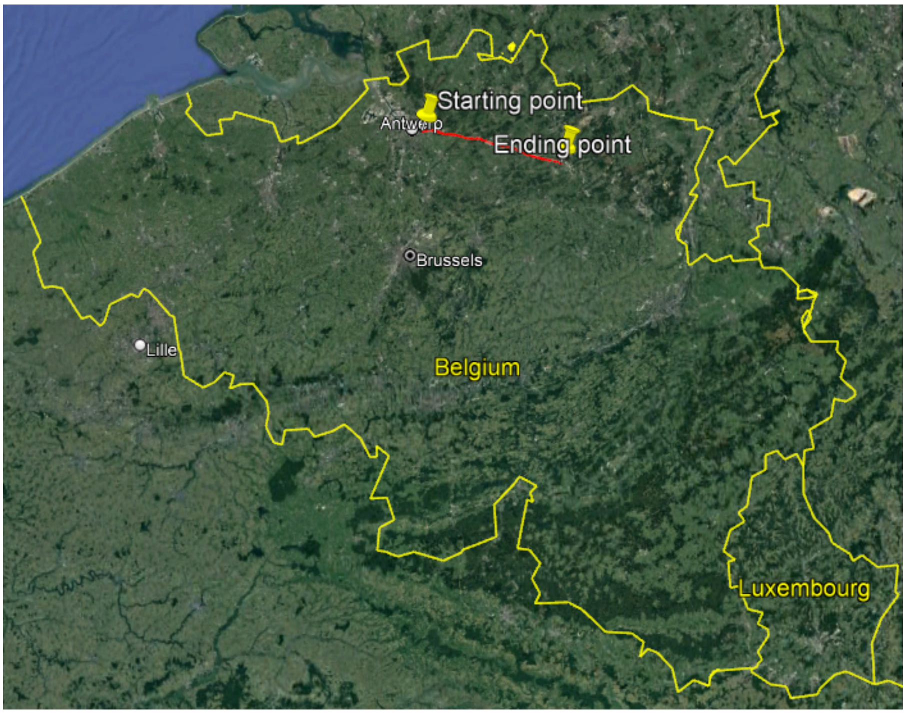
Starting point
Antwerp
Ending point
Brussels
Lille
Belgium
Luxembourg

FIGURE 2.1: Network position in Belgium

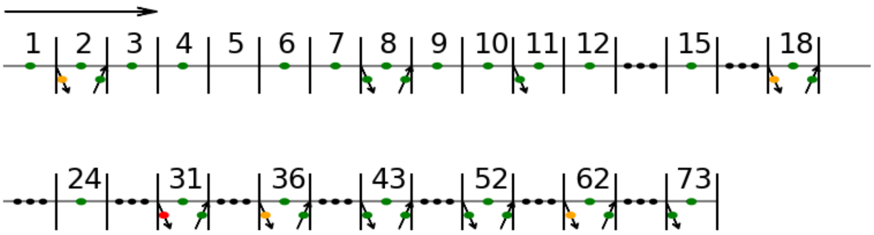
1
2
3
4
5
6
7
8
9
10
11
12
15
18
24
31
36
43
52
62
73

FIGURE 2.2: Selected network stretch

The sensors' colours represent:
● functional sensors
● failing sensors
● sensors giving faulty measurements
●●● multiple consecutive empty segments
and no dot signifies an empty segment.
Above each non-empty segment, its number is depicted.
Each coloured dot represents a group of sensors.

The selected stretch consists of 82 sensors, all measuring vehicle speed and traffic flow. The sensors are placed per lane, meaning that each sensor measures data for one lane, and that in a vertical "slice" of the road, there are, and should be, as many sensors as lanes. The stretch is split in segments of 400m - 700m long, so that the estimation product can be accurate. Each segment is taken in this range, so that at maximum only one mainstream and/or one ramp can lie there. This means that a segment can contain one mainstream, or one ramp, or one mainstream and one ramp, or it can be empty. Each segment's length, along with its distance from the beginning of the stretch plus its own length, are listed in Table 2.1. Note that the entire Antwerp network does not yet contain the infrastructure needed in order to receive reported speed by connected vehicles, so the flow spot-detectors also measure speed. It is highlighted that the estimator is a cross-lane estimator that utilizes aggregated measurements per segment. So, we aggregate the per-lane measurements, so as to consider one measurement per segment. So, the number of sensor groups is 38.

Considering Figure 2.2, it should be noted that this highway stretch requires the measurement of the mainstream flow of one segment between segments 2 and 15, then 18 or 24, then 31 and then one measurement between 36 and 52. Note that, the off-ramp that gives faulty measurements in segment 62 does not require an additional measurement, because there is not any consecutive orange or red ramp after it and, of course, because the mainstream flow of segment 73 is measured for system observability. So, the partial ramp-flow availability case applies.

2.4 TRAFFIC DATA COLLECTION ALGORITHM

In order to collect the data from the motorway stretch of the Antwerp network, process it and pass it to the estimator, an algorithm shown in Figure 2.3 was developed and implemented in Matlab.

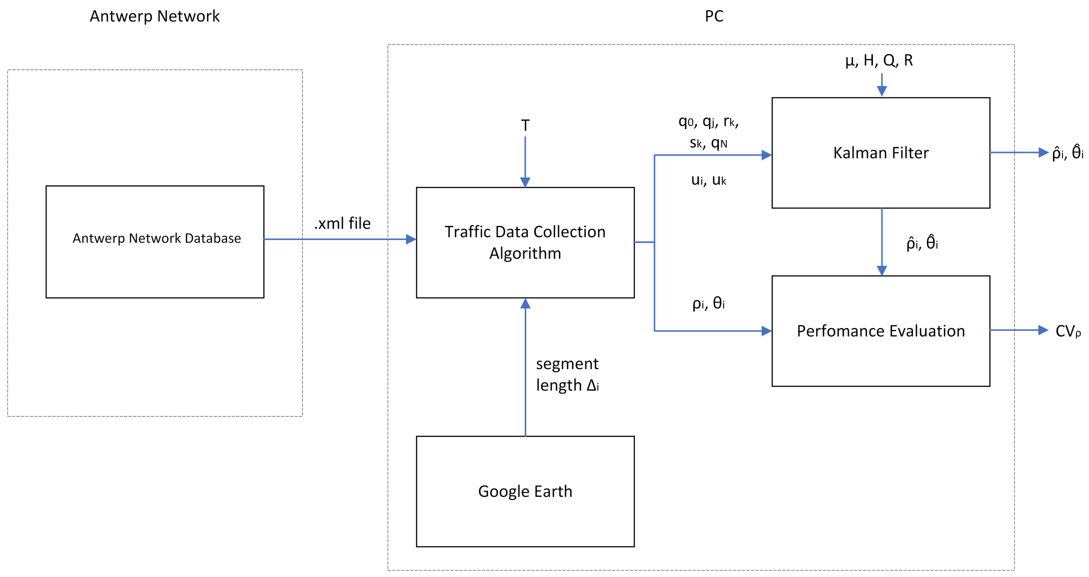
Antwerp Network
PC
Antwerp Network Database
.xml file
T
Traffic Data Collection Algorithm
segment length Δi
Google Earth
μ, H, Q, R
q0, qj, rk, sk, qN
ui, uk
Kalman Filter
ρ̂i, θ̂i
ρ̂i, θ̂i
ρi, θi
Perfomance Evaluation
CVρ

FIGURE 2.3: Setup diagram

No.	Length (km)	Length so far (km)
1	0.6	0.6
2	0.5	1.1
3	0.7	1.8
4	0.7	2.5
5	0.7	3.2
6	0.7	3.9
7	0.55	4.45
8	0.7	5.15
9	0.7	5.85
10	0.7	6.55
11	0.7	7.25
12	0.7	7.95
13	0.7	8.65
14	0.7	9.35
15	0.7	10.05
16	0.7	10.75
17	0.7	11.45
18	0.43	11.88
19	0.7	12.58
20	0.7	13.28
21	0.7	13.98
22	0.7	14.68
23	0.7	15.38
24	0.7	16.08
25	0.7	16.78
26	0.7	17.48
27	0.7	18.18
28	0.7	18.88
29	0.7	19.58
30	0.43	20.01
31	0.5	20.51
32	0.7	21.21
33	0.7	21.91
34	0.7	22.61
35	0.4	23.01
36	0.5	23.51
37	0.7	24.21
38	0.7	24.91
39	0.7	25.61
40	0.7	26.31
41	0.7	27.01
42	0.4	27.41
43	0.5	27.91
44	0.7	28.61
45	0.7	29.31
46	0.7	30.01
47	0.7	30.71
48	0.7	31.41
49	0.7	32.11
50	0.7	32.81
51	0.7	33.51
52	0.7	34.21
53	0.6	34.81
54	0.7	35.51
55	0.7	36.21
56	0.7	36.91
57	0.7	37.61
58	0.7	38.31
59	0.7	39.01
60	0.7	39.71
61	0.5	40.21
62	0.4	40.61
63	0.7	41.31
64	0.7	42.01
65	0.7	42.71
66	0.7	43.41
67	0.7	44.11
68	0.7	44.81
69	0.7	45.51
70	0.7	46.21
71	0.7	46.91
72	0.7	47.61
73	0.4	48.01
	-	

TABLE 2.1: Segment characteristics

This algorithm uses a periodic timer, which fires every one minute to download an xml file, containing data from a small database with real-time measurements from all sensors of the entire Antwerp network. For each sensor inside the selected stretch, the algorithm cleans a lot of unuseful-for-the-purpose data, while keeping only its unique ID and for every class: its flow, its arithmetic speed and its harmonic speed. A class $\in \{1, 2, 3, 4, 5\}$ describes the type of vehicle that may pass a lane. Table 2.2 shows which class corresponds to which vehicle type.

Class	Vehicle length (m)	Vehicle types
1	0.0-1.0	Motorbikes
2	1.0-4.9	Cars
3	4.9-6.9	Vans
4	6.9-12.0	Rigid Lorries
5	>12.0	(Semi-)Trailers or Busses

TABLE 2.2: Class number per vehicle length and type

Due to the fact that the Kalman filter used is applied across all existing lanes in each segment and not to each one individually, the algorithm calculates the sum of the flows and the average weighted arithmetic speeds of all the classes of all the adjacent sensors inside a segment, categorized by their position (i.e. mainstream, on-ramp, off-ramp). For instance, let us consider a segment i, which contains 4 lanes, at the point where the sensors are placed. This means that there are at maximum (the maximum is and should be the most common case, in the sake of correct results) 4 sensors, that is, one per lane: a, b, c and d. The sensors should not be ahead or behind the other sensors, but they must all be arranged vertically in a straight line, so that no vehicle that changes lane is measured twice or more. Each sensor takes 5 simultaneous measurements, one for each class. So, the flow is calculated as a summation of flow of class j of sensor s (one sensor in a lane), $j \in \{1, 2, 3, 4, 5\}$, $s \in \{a, b, c, d\}$. The same idea applies to the calculation of speeds, but instead of summation, taking the weighted average of arithmetic speed of class j of sensor s is needed. It is reminded that the Antwerp network uses lane sensors, so taking each adjacent lane's measurements and aggregating them into one measurement is the only reasonable option for feeding the filter.

It should be noted that sometimes, especially - but not only - at late hours, the road is empty, with no vehicles passing for one or several minutes. In that case the measurements taken are 0 for the speed and 0 for the flow (or rarely even negative values). So, for zero measurements, we simply equate the new value with the previous one, for consistency. Note that for the initial values being zero (speed, flow of the first minute measured), we assign the value 120 km/h (the usual European speed limit) for zero or negative speeds and 0 veh/h for negative flows.

In the case where there are no speed measurements available (the filter is for segment flows, or equivalently segment densities, not for segment speeds), linear interpolation is used with the outer coordinates being the last and the next functional segments' speeds. For instance, in the selected highway stretch, segments 16-17 are empty, so, interpolation between mainstream sensors 15 and 18 is needed in order to find the speeds.

Then, after transforming the motorway stretch into a data structure consisting of segment elements and creating the necessary input files, it is time to run the estimator.

It should not be omitted that, in Figure 2.3, T is the detection interval of the flow sensors, r_k and s_k are measured on-ramp and off-ramp flows, u_i and u_k are mainstream and measured ramp speeds and the segmentation process along with each segment's Δ_i are both automatically received from Google Earth by mapping the chosen segmentation onto the actual map.

2.5 PARAMETER TUNING

To evaluate the accuracy of the estimation results, a performance index is needed. The performance index used is known from statistics as Coefficient of Variation CV_ρ of the estimated density $\hat{\rho}_i$, with respect to the ground truth density ρ_i [1].

$$CV_\rho = \frac{\sqrt{\frac{1}{KN}\sum_{k=1}^{K}\sum_{i=1}^{N}[\hat{\rho}_i(k) - \rho_i(k)]^2}}{\frac{1}{KN}\sum_{k=1}^{K}\sum_{i=1}^{N}\rho_i(k)} \tag{2.25}$$

where $N = 73$ is the total number of segments of the motorway and K is the total time (in minutes) used. The index k runs from 1 to $K = 720$ from 8 AM to 8 PM ($(20-8) \times 60 = 720$), which is the time interval chosen to be shown.

The numerator is the standard deviation of $\hat{\rho}_i(k)$, or else its Root-Mean-Square Error, and the denominator is the mean of $\rho_i(k)$. CV_ρ compares the degree of variation from the $\hat{\rho}$ data series to the ρ data series. The higher the CV_ρ, the greater the dispersion. Thus, this index should be kept as small as possible.

In order to employ the estimator, its parameters must be appropriately tuned. In the following experiments, the sensitivity of the estimation scheme to the values of the filter parameters Q and R is evaluated. The entry of matrix Q for the density is equal to $\sigma_Q \times I_N$, while the entry of Q for the unmeasured ramps is equal to $\sigma_{Q_{Un}} \times I_{l_r+l_s}$. Similarly, matrix R is equal to $\sigma_R \times I_{l_r+l_s}$. CV_ρ is compared every time by varying (empirically) one of these three σ values by orders of magnitude, while keeping the other two constant. The results in Figures 2.4, 2.5, 2.6 prove that the performance index is highly insensitive to the change of the values of the filter parameters from 10^{-3} to 10^2, but for any σ being equal to 10^3 it is being lowered by approximately 10% than the 10^{-3} value. For powers greater than 3, the σ_Q and $\sigma_{Q_{Un}}$ values show the exact same behaviour, while the behaviour of σ_R is very interesting as it decreases almost 50% from its 10^{-3} value and at the power of 10, it increases again by approximately 66% from the 10^9 case. Nonetheless, in CV_ρ absolute % values, the percentage difference from the worst case to the best, is just a mere 1.4% for σ_R. From here on, the triplet $\{\sigma_Q = 1, \sigma_{Q_{Un}} = 0.1, \sigma_R = 100\}$ is kept.

Moreover, the initial values μ (2.23), that correspond to density, are set equal to 15, while entries that correspond to unmeasured ramps are set to 5 and $H = I_{(N+l_r+l_s)}$ (2.24). These initial values impact the estimation results only when the filter is switched on, that is, for a very short amount of time, and thus practically insignificant. For instance, one should look at segment 9 of Figure 2.14, where it is evident how quickly the estimation values approach the real ones.

The measurements for producing the CV_ρ Figures 2.4, 2.5 and 2.6 were taken as a mean of measurements from Wednesday 4/1/2023 to Tuesday 10/1/2023, that is, 7 days. From these days, only Saturday 7 and Sunday 8 were without any sign of congestion.

In general, the penetration rate, that is, the percentage of total vehicles that are connected, may differ from 0 to 100%. In this thesis, it is assumed that the penetration rate is 100%, as the speeds are being received in real-time from sensor measurements. So, for a penetration rate smaller than this, CV_ρ would be greater.

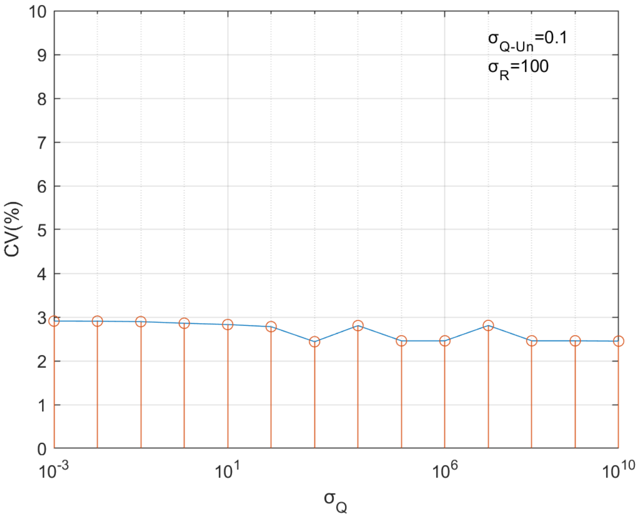

FIGURE 2.4: CV_ρ considering various powers of the σ_Q filter parameter

2.6 ESTIMATION RESULTS

The point of developing a real-time traffic estimation algorithm is traffic monitoring and control. Thus, the algorithm proves its meaningfulness, when there is traffic, that is, at specific days and hours. The six speed Figures 2.7, 2.8, 2.9 and the six flow Figures 2.10, 2.11, 2.12 depict the average weighted speed (weighted arithmetic mean of the speeds) and the total flow (sum of the flows) of the real sensor groups 12, 13, 14, 15, 16 and 17 (segments 9-15), on Thursday 22 September 2022. Plainly, the measurements are noisy.

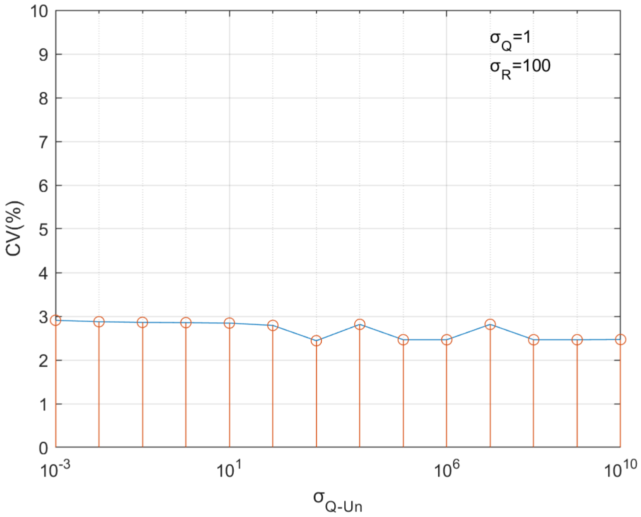

FIGURE 2.5: CV_ρ considering various powers of the $\sigma_{Q_{Un}}$ filter parameter

It is clear from the Figures that congestion has been created around 9 AM and 12 AM. The congestion begins in one of the 24th-31st segments (confirmed congestion from the density graph is last seen at the 21st sensor group - segment 24, next confirmed free-flow conditions are firstly seen at the 23rd sensor group - segment 31) and gradually spills back to the 6th segment (7th sensor group). The drops in the speeds and the flows are forcing the vehicles "trapped" inside to form a long queue for many segments back (spillback), that is, for many kilometers. As seen in density graph 2.15, no congestion has been recorded from the mainstream sensor of segment 31. On the contrary, the density between the critical hours has dropped and the flow of segment 24 takes a really hard drop of approximately 2000 veh/h in just 4 minutes (see Figure 2.13), so we assume that an incident took place between segment 24 and the off-ramp in segment 31, blocking one of the two existing lanes there. Clarifying, Figure 2.13 depicts the flow, density, the fundamental diagram and the speed of segment 24 on 22/09/2022, for each hour of the day. The fundamental diagram shows the relationship between traffic flow (veh/h), traffic density (veh/km), and speed (km/h) under different traffic conditions. At low traffic densities, the speed is relatively high, and the traffic flow is smooth. As traffic density increases, the speed starts to decrease, indicating congestion, and the flow may still increase, but at a slower rate. At very high traffic densities, the speed drops significantly, approaching zero, and the traffic flow reduces drastically, indicating a traffic jam or standstill.

Also, an interesting point is extracted by looking at, for instance, 4/1/2023, segment 24 in Figure 2.16. As soon as there is congestion, the estimator quickly tracks the ground truth values. But the congestion lasts for too little, so the estimator does not perfectly reach the sharply formed peak, as this is not feasible in estimating applications. This can also be seen on 22/9/2022, segment 15 in Figure 2.14, where the flow largely forms peaks that last too little. But looking at a Figure in which the congestion lasts, (e.g. 5/1/2023,

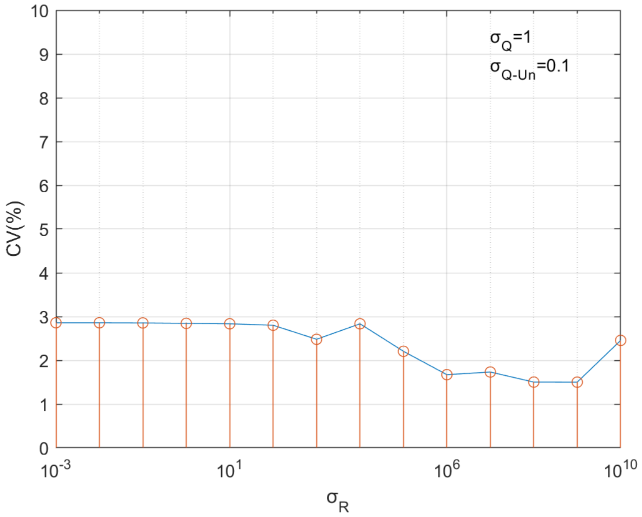

FIGURE 2.6: CV_ρ considering various powers of the σ_R filter parameter

segment 24 in Figure 2.17), the estimator quickly catches up.

Observing each one of Figures 2.14, 2.15, 2.16, 2.17, there is always the warm-up period in the beginning of each day, when the estimator takes about half an hour to start to successfully track the ground truth's trajectory. It should be clarified that, in this thesis, each day was separately sampled. In a real application, the estimator would be running continuously, so the warm-up period would happen only once, at the first use of the estimator.

Regarding the density values at the first 7 kilometers in Figures 2.18, 2.19, 2.20, 2.21, it is clear from Figure 2.1 that the beginning of the selected stretch is very close to the main city of Antwerp, so there is, understandably, more traffic there.

In total, data for 24 days were sampled in real time, but only some of the congested days are utilized and presented in the Figures below.

Concluding, the estimator produces traffic state (density) estimation values. From the density - time Figures 2.14, 2.15, 2.16, 2.17 and heatplots of density over space and time 2.18, 2.19, 2.20, 2.21 for the days 22/9/2022, 4-6/1/23, it is evident that for either congested traffic, or free-flow traffic, the proposed estimation scheme successfully estimates and dynamically tracks density in both time and space, given correct input.

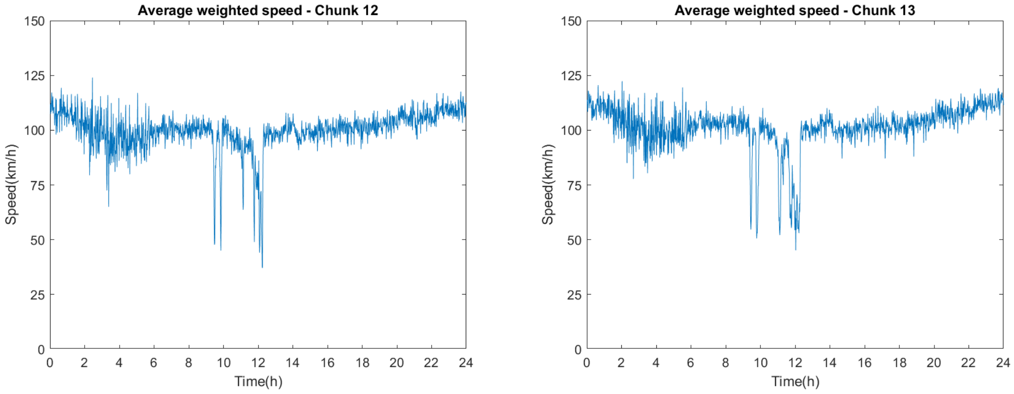

FIGURE 2.7: Average weighted speeds of real sensor groups 12-13 in km/h on 22/9/2022

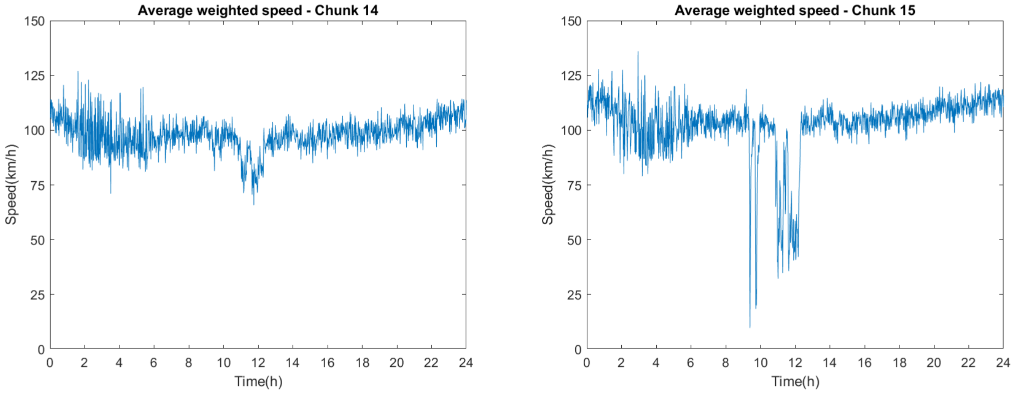

FIGURE 2.8: Average weighted speeds of real sensor groups 14-15 in km/h on 22/9/2022

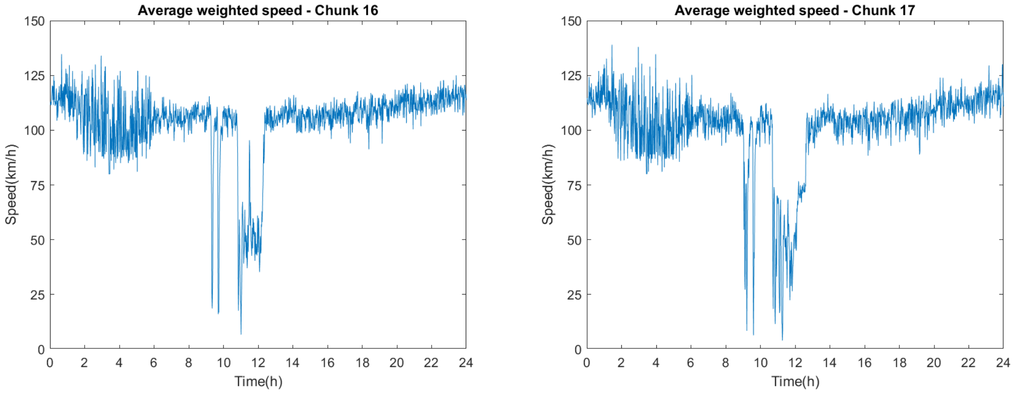

FIGURE 2.9: Average weighted speeds of real sensor groups 16-17 in km/h on 22/9/2022

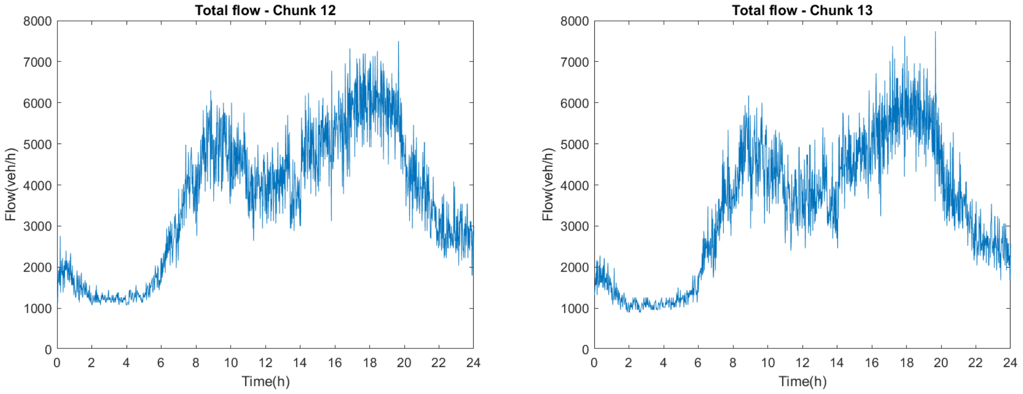

FIGURE 2.10: Total flows of real sensor groups 12-13 in veh/h on 22/9/2022

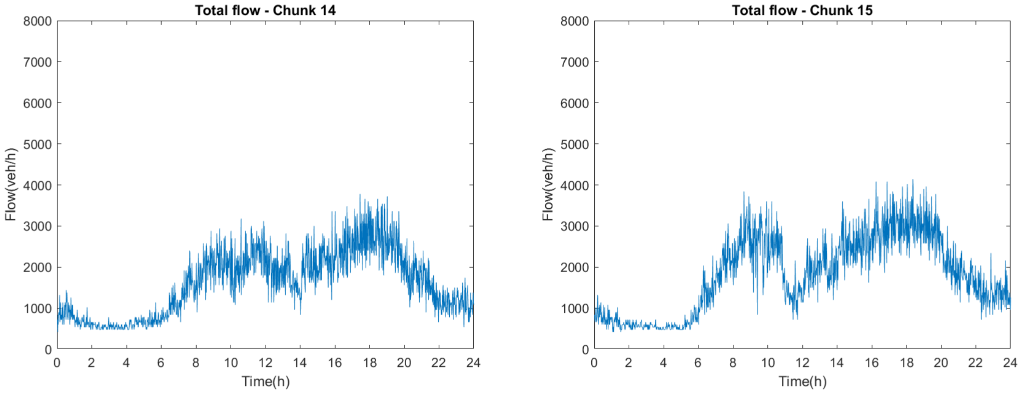

FIGURE 2.11: Total flows of real sensor groups 14-15 in veh/h on 22/9/2022

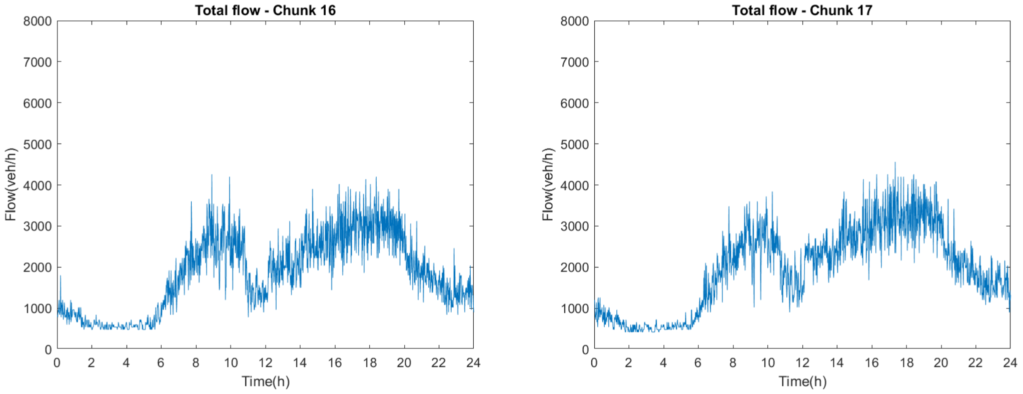

FIGURE 2.12: Total flows of real sensor groups 16-17 in veh/h on 22/9/2022

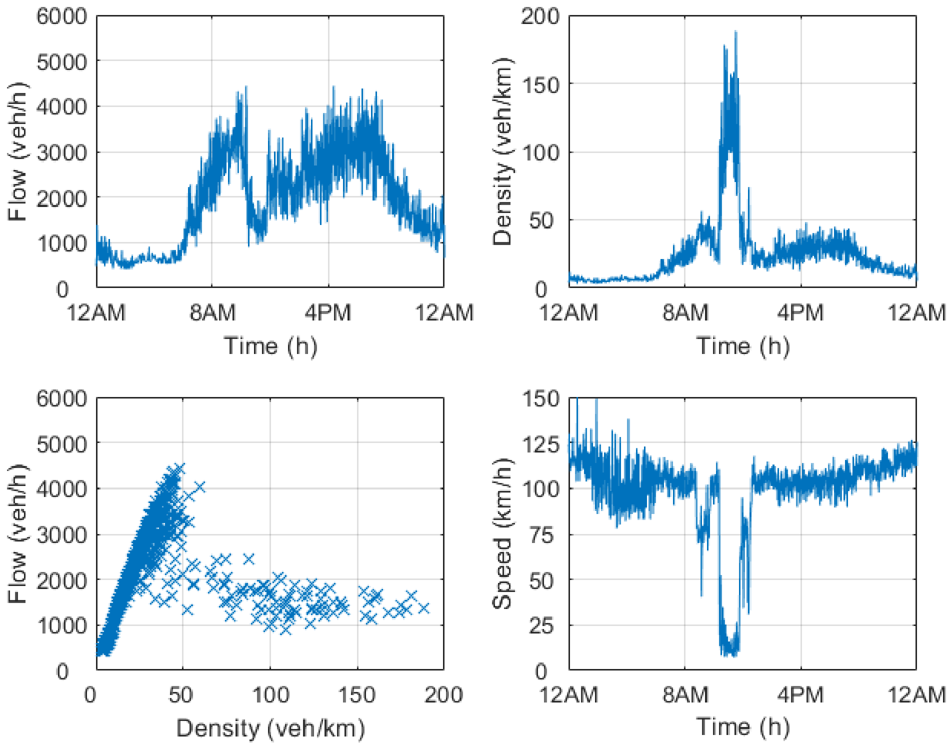

FIGURE 2.13: Flow, Density, Fundamental Diagram and Speed of segment 24 on 22/9/2022

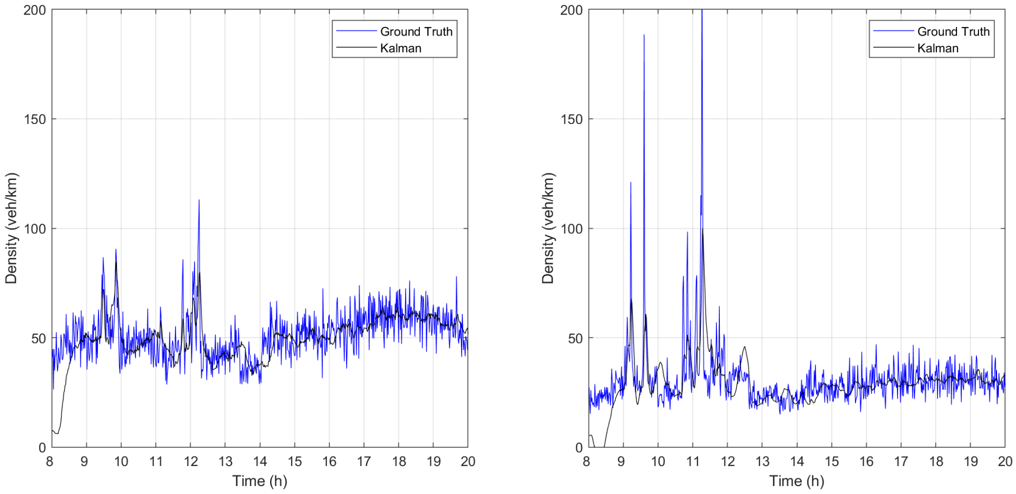

Segment 9

Segment 15

FIGURE 2.14: Comparison between ground truth (blue line) and estimated (black line) traffic density at segments 9 and 15 for 22/09/2022

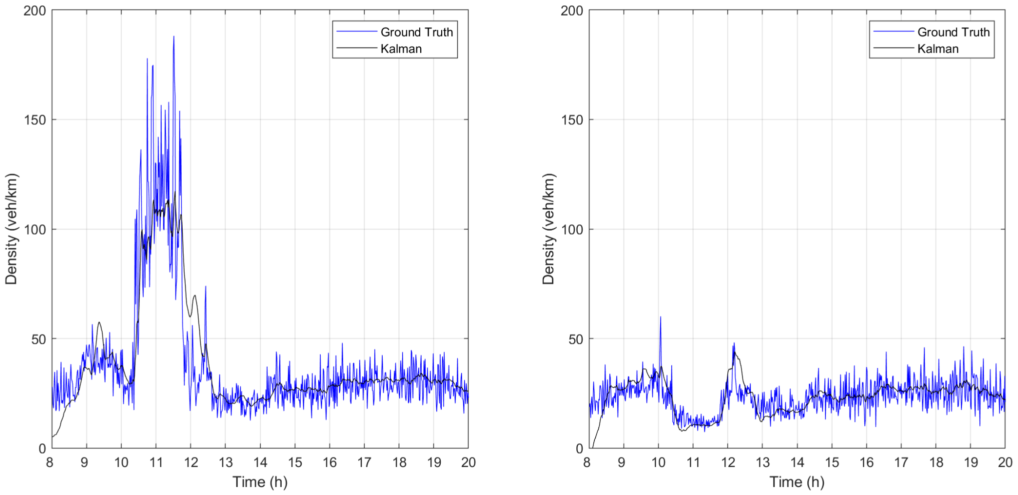

Segment 24

Segment 31

FIGURE 2.15: Comparison between ground truth (blue line) and estimated (black line) traffic density at segments 24 and 31 for 22/09/2022

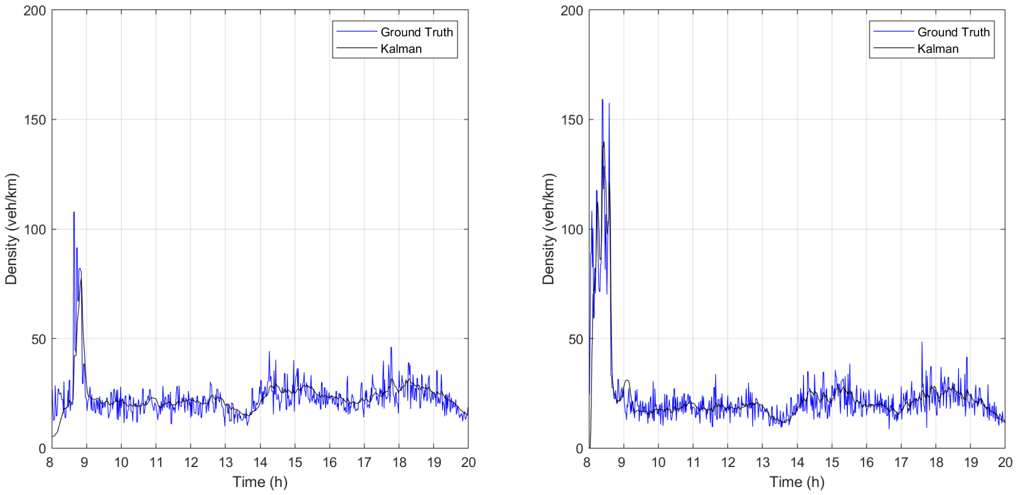

Segment 24

Segment 31

FIGURE 2.16: Comparison between ground truth (blue line) and estimated (black line) traffic density at segments 24 and 31 for 04/01/2023

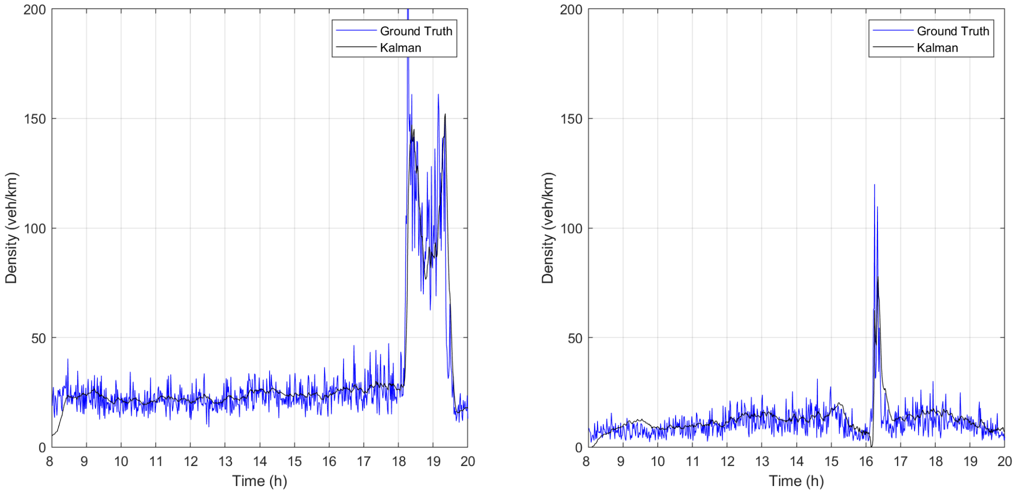

Segment 24 Segment 62

FIGURE 2.17: Comparison between ground truth (blue line) and estimated (black line) traffic density at segment 24 for 05/01/2023 (left) and at segment 62 for 06/01/2023 (right)

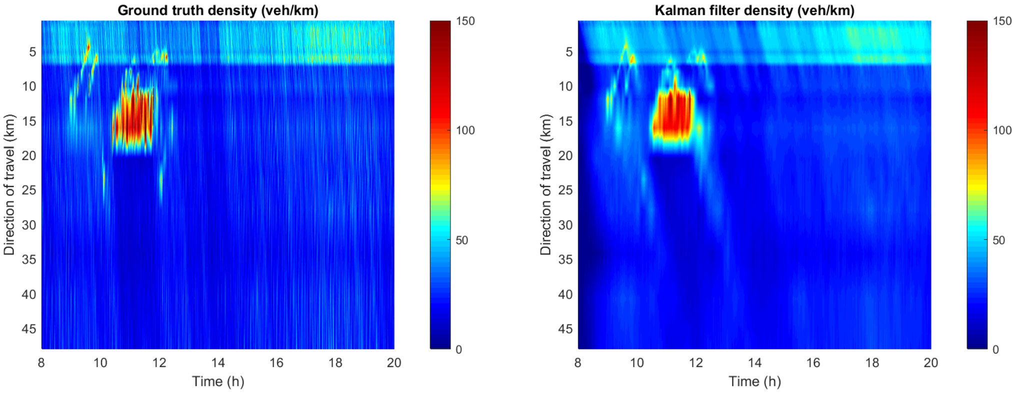

Ground Truth Kalman Estimation

FIGURE 2.18: Comparison between real (left) and estimated (right) density for Thursday 22/09/2022

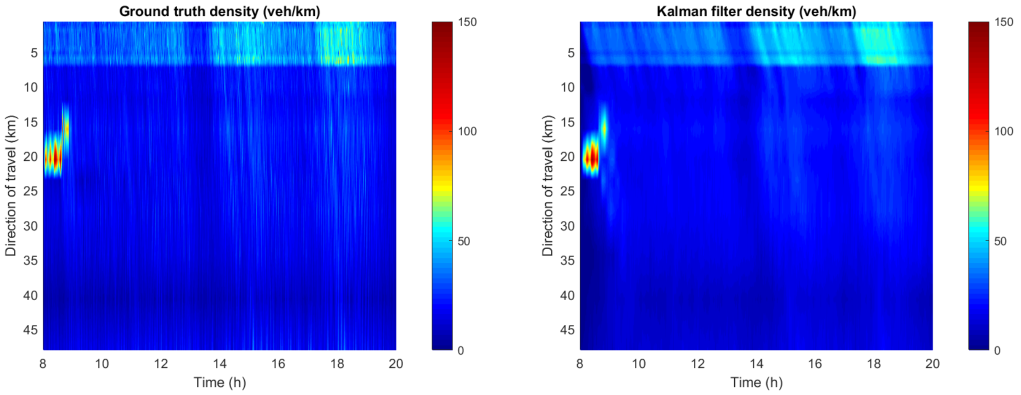

Ground Truth

Kalman Estimation

FIGURE 2.19: Comparison between real (left) and estimated (right) density for Wednesday 04/01/2023

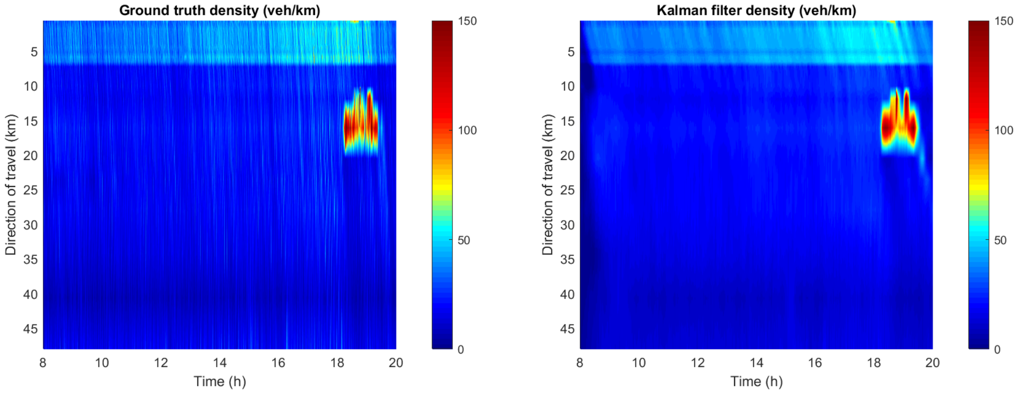

Ground Truth

Kalman Estimation

FIGURE 2.20: Comparison between real (left) and estimated (right) density for Thursday 05/01/2023

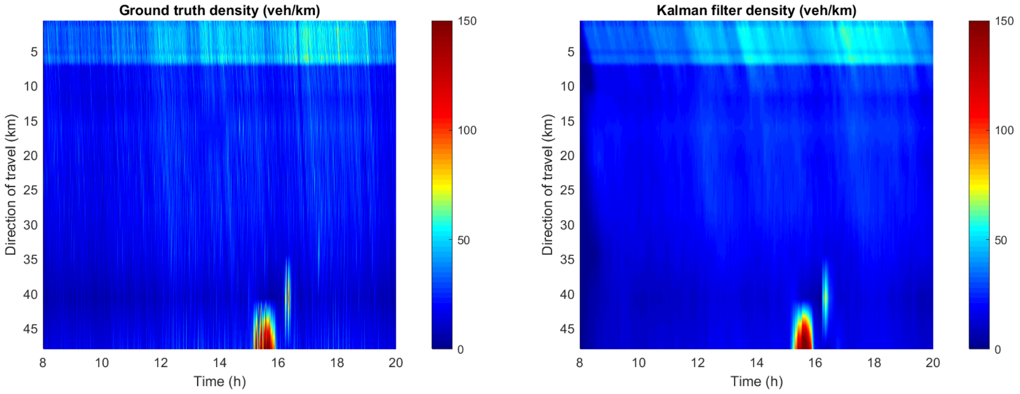

Ground Truth

Kalman Estimation

FIGURE 2.21: Comparison between real (left) and estimated (right) density for Friday 06/01/2023

CHAPTER 3

HIGHWAY TRAFFIC CONTROL WITH ACC-VEHICLES

3.1 THE AIMSUN NEXT MICROSCOPIC SIMULATOR

Advanced Interactive Microscopic Simulator for Urban and Non-urban Networks (AIMSUN), or most commonly known as Aimsun Next [6], is a commercial microscopic traffic simulation software vastly used by transport researchers and professionals. This tool provides different types of road, like highway, pedestrian, railway, etc, vehicle types, like cars, trucks, trams, buses, bicycles, even pedestrians, and most traffic equipment, like traffic lights, traffic detectors, Variable Message Signs, etc.

The input data required by the microsimulator is a simulation scenario with a set of simulation parameters, like simulation time, reaction time, statistics interval etc, that compose an experiment. Each experiment can have one or more simulation replications, because each replication is affected by stochasticity. So, in order for accurate conclusions to be drawn, many replications of an experiment are needed. A scenario also requires to be fed with traffic demand (veh/h), network characteristics, road type(s), vehicle type(s) and driving behavior(s). Inputs, like traffic control plans and percentage of vehicles with ACC/CACC capability, are not required, but are the essence of this thesis and thus, are used. Common outputs produced at the end of a simulation are macroscopic measurements, like total time spent in the network, average delay time of a vehicle, a section's flow, density etc.

The Aimsun Next microscopic simulator consists of an API and a microSDK. All aforementioned inputs and outputs can be inserted and extracted, respectively, from the API's GUI, but for details, like changing some factors with logic, a C++, or a Python, solution (.sln) file is best. The microSDK is used as a tool for integrating new behavioral models, like the car-following, the lane-changing, the gap-acceptance and others and, if desirable, overriding the default ones. The new models can also be implemented with logic and in specific sections and lanes.

3.2 BEHAVIORAL MODELS

A variety of distinct sub-models are included in traffic microsimulation models, that try to address various characteristics of the human driver. The car-following and lane-changing models are the two most crucial sub-models in a traffic simulation system.

3.2.1 CAR-FOLLOWING MODEL

In order to represent the relative positions of vehicles as measured in time and space, various terminology used in traffic flow theory, and also in the Aimsun Next tool, must first be specified. All of the following theory is explicitly specified in Aimsun Next's manual [6].

- **Headway**: The time between the front bumper of a vehicle and the front bumper of the following vehicle
- **Gap**: The time between the rear bumper of a vehicle and the front bumper of the following vehicle
- **Spacing**: The space between the front bumper of a vehicle and the front bumper of the following vehicle
- **Clearance**: The space between the rear bumper of a vehicle and the front bumper of the following vehicle

These will be used in the following description of vehicle behavior.

The Aimsun Next tool uses the Gipps car-following model [7]. This model includes parameters that are determined by local parameters, which depend on the "type of driver", each section's geometry, the influence of vehicles on adjacent lanes, etc.

Acceleration and deceleration are this model's two components. The acceleration phase is when the vehicle tries to catch up to a specific desired speed, so it accelerates. The deceleration phase is when the a vehicle has to slow down due to its leader vehicle's behaviour.

Based on this model, the maximum speed to which a vehicle n can accelerate during a time period $(t, t + dt)$ is:

$$V_a(n, t + dt) = V(n, t) + 2.5a(n)dt\left(1 - \frac{V(n,t)}{V^*(n)}\right)\sqrt{0.025 + \frac{V(n,t)}{V^*(n)}} \tag{3.1}$$

where:
-$V_a(n, t)$ is the speed of vehicle n at time t
-$V^*(n)$ is the desired speed of vehicle n for the current section
-$a(n)$ is the maximum acceleration for vehicle n, a fixed value
-dt is the simulation cycle
-constant values come from an initial calibration of the model

At the same time, the maximum speed that n can reach during the time interval $(t, t + dt)$, according to its own characteristics and the limitations imposed just by the presence of the leading vehicle (vehicle $n - 1$) is:

$$V_b(n, t + T) = d(n)T +$$

$$\sqrt{d(n)^2T^2 - d(n)\sqrt{2(x(n-1,t) - s(n-1) - x(n,t)) - V(n,t)T - \frac{V(n-1,t)^2}{d'(n-1)}}} \tag{3.2}$$

where:
-$d(n)$ (< 0) is the maximum deceleration chosen from a normal distribution for vehicle n
-$x(n,t)$ is the position of the front bumper of vehicle n at time t
-$x(n-1,t)$ is the position of the front bumper of the preceding vehicle $n-1$ at time t
-$s(n-1)$ is the length of vehicle $n-1$
-$d'(n-1)$ is an estimation of vehicle's ($n-1$) desired deceleration
-$x(n-1,t) - s(n-1) - x(n,t)$ is the clearance between vehicles n and $n-1$
-T is the reaction time

So, the speed for vehicle n during time interval $(t, t+dt)$ is:

$$V(n,t+dt) = \min\{V_a(n,t+dt), V_b(n,t+dt)\} \tag{3.3}$$

Then, the n^{th} vehicle's speed is utilized in order to update the position of the same vehicle in its present lane. The acceleration phase is integrated using the rectangle method corresponding to the following equation:

$$x(n,t+dt) = x(n,t) + V(n,t+dt)dt \tag{3.4}$$

while the deceleration phase integration uses the trapezoid method following this equation:

$$x(n,t+dt) = x(n,t) + 0.5(V(n,t) + V(n,t+dt))dt \tag{3.5}$$

The minimum headway (minimum distance) between the leader vehicle and follower vehicle is a constraint of the vehicle's deceleration, and thus, it is applied.
The minimum headway constraint is being utilized as:
If

$$x(n-1,t+T) - [x(n,t) + V(n,t+T)T] < V(n,t+T) \times MinHW(n) \tag{3.6}$$

then

$$V(n,t+T) = \frac{x(n-1,t+T) - x(n,t)}{MinHW(n) + T} \tag{3.7}$$

where
-$x(n,t)$ is the position of the front bumper of vehicle n at time t
-$x(n-1,t)$ is the position of the front bumper of the preceding vehicle $n-1$ at time t
-$MinHW(n)$ is the minimum headway of vehicle n between itself and vehicle $n+1$

Each vehicle type is given the ability to estimate it's leader's deceleration using the Sensitivity Factor parameter α. So, for a vehicle n the estimation of the maximum deceleration $d(n-1)(<0)$ desired by vehicle $n-1$ is:

$$d'(n-1) = d(n-1) \times \alpha \tag{3.8}$$

- When $\alpha = 1$, the model functions purely as the Gipps model.
- When $\alpha < 1$, vehicle n underestimates the deceleration of vehicle $n-1$ and thus, vehicle n becomes more imprudent, closing the distance (space-gap) with vehicle $n-1$.
- When $\alpha > 1$, the vehicle overestimates the deceleration of vehicle $n-1$ and thus, n becomes more conservative, opening the distance (gap) vehicle $n-1$.

Figure 3.1 depicts the three sensitivity factor types based on their value ($\alpha = 1$, $\alpha < 1$, $\alpha > 1$) and their impact on traffic, with the blue dots representing vehicles on a road.

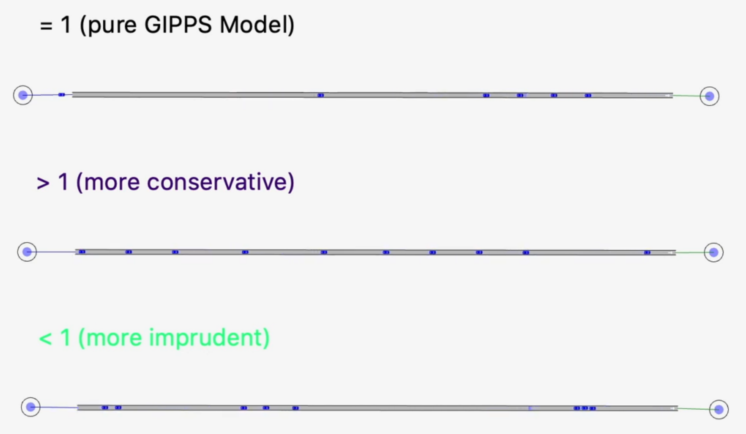

FIGURE 3.1: Sensitivity factor types and their impact

MODIFIED MODEL FOR CONGESTED HIGHWAYS

The Gipps car-following model's estimated speed for high densities does not correspond to the speeds observed in roads with real congestion. The dependence of speed is modified as a function of density using a modified model. So, the clearance equation will be transformed as follows.

The Gipps equation for the clearance between n and $n-1$ is:

$$\begin{aligned} Clr(t) &= (x(n-1,t) - x(n,t) - s(n-1)) \\ &= \frac{V(n-1,t)^2}{2d(n-1)} - \frac{V(n,t)^2}{2d(n)} + (0.5V(n,t) + V(n,t+T))T \end{aligned} \tag{3.9}$$

which is transformed to:

$$
\begin{aligned}
Clr(t) = \frac{V(n-1,t)^2}{2d(n-1)} - \frac{V(n,t)^2}{2d(n)} + (1-b)((0.5V(n,t)+V(n,t+T))T) \\
+ b((0.5V(n,t)+V(n,t+T))\left(\sqrt{\frac{V(n,t)}{V_{desired}}}T\right)
\end{aligned}
\tag{3.10}
$$

$$
\begin{aligned}
V(n,t+T) = d(n)T^* \\
+ \sqrt{(d(n)T^*)^2 - d(n)\left[2Clr(t) - V(n,t)T^* - \frac{V(n-1,t)^2}{d(n-1)}\right]}
\end{aligned}
\tag{3.11}
$$

where

$$
T^* = T\left(1 + b\left(1 - \sqrt{\frac{V(n,t)}{V_{desired}}}\right)\right) \tag{3.12}
$$

ADAPTIVE CRUISE CONTROL (ACC) CAR-FOLLOWING

Adaptive cruise control (ACC) is a type of advanced driver-assistance system for road vehicles, that automatically adjusts the vehicle's desired speed and its desired time-gap, when following a slower vehicle, in order to maintain a safe distance from it [3]. Control is based on sensor data from on-board equipment, like a radar, laser sensor, or camera configuration, that allows the vehicle to brake, when it notices another vehicle is approaching up ahead and accelerate when traffic permits. These systems impose automatically the calculated acceleration or deceleration to the subject vehicle, based on real-time measurements and driver parameterisation. In Aimsun Next, the ACC option consists of two modes:

- Speed Regulation mode: $a_{sv} = k_1 \cdot (V_f - V_{sv})$
  where:
  - a_{sv}: acceleration recommended by the ACC controller to the subject vehicle ($\frac{m}{sec^2}$)
  - k_1: gain in the speed difference between the free-flow speed and the subject vehicle's current speed (sec^{-1})
  - V_f: free-flow speed ($\frac{m}{sec}$)
  - V_{sv}: current speed of the subject vehicle ($\frac{m}{sec}$)
- ACC Gap Regulation mode: $a_{sv} = k_2(d - L - t_{hw}V_{sv}) + k_3(V_l - V_{sv})$
  where:
  - a_{sv}: acceleration recommended by the ACC controller to the subject vehicle ($\frac{m}{sec^2}$)

- k_2: gain on position difference between the preceding vehicle and the subject vehicle (sec^{-2})
- k_3: gain on speed difference between the preceding vehicle and the subject vehicle (sec^{-1})
- d: distance between the subject vehicle's front bumper and the preceding vehicle's front bumper, or $x(n-1) - x(n)$ with the previous notation (m)
- t_{hw}: desired time gap of the ACC controller (sec)
- V_{sv}: current speed of the subject vehicle ($\frac{m}{sec}$)
- L: length of the preceding vehicle, or $s(n-1)$ with the previous notation (m)
- V_l: current speed of the preceding vehicle ($\frac{m}{sec}$)

Speed Regulation Mode is used, when no vehicle is ahead of the current vehicle, or if the vehicle ahead is too far. Else, ACC Gap Regulation mode is used. ACC systems are made to provide more safety and comfort, hence some ACC parameters may be conservative, that is, comparatively large time-gaps and low accelerations. Nevertheless, such conservative parameter values may lead to degradation of the static and dynamic road capacity compared to manual-driving vehicle traffic. The higher the penetration rate of ACC-equipped vehicles, the more pronounced will be the influence of their driving style [8].

3.2.2 LANE-CHANGING MODEL

Changing lane is a determinant of traffic flow. So, modeling it is critical in forming a congestion in a microscopic simulator. The default lane-changing model in the Aimsun Next microscopic simulator is the Gipps lane-changing model [9]. The Gipps lane-changing model makes a decision based on the gap acceptance principle. In the ramp merging case, a vehicle that wants to merge into the mainstream lane from the acceleration lane looks for a gap, which is safe, and will not cause a collision, otherwise it waits for such a gap. The Gipps lane-changing model is too conservative against real ramp merging procedures in a way that it causes low merging success rates. On the contrary, the closer vehicles are to the end of the acceleration lane, the more they desire to change lane. So, being at the end of the acceleration lane and still not having managed to change lane means that the driver is probably going to accept more tough and stressful gap conditions. In this thesis, a heuristic forced lane-changing model developed in [10] is utilized, overwriting the default one, in order to create the ability of forming ramp merging congestion and the capacity drop phenomenon.

In general terms, congestion is a formed queue of vehicles that move at low speeds. Congestion can be categorized into stop-and-go waves and standing queues. In this thesis, the research concerns standing queues. In a standing queue, the head is fixed at an active bottleneck. This means that there is traffic jam upstream of the bottleneck and free-flow conditions downstream. In theory, downstream of an active bottleneck, the outflow of this queue should be equal to the capacity. But in spite of that, the discharge flow downstream of the bottleneck may be lower than capacity. This is the capacity drop phenomenon [11]. This happens because *i*) all vehicles in congestion move slowly at pretty much the same speed, without leaving any space for overtaking or lane changing and *ii*) vehicles with a slower speed preference start slower, with the result being the prolongation of the congestion [12].

GIPPS LANE-CHANGING MODEL

The following theory is explicitly specified in Aimsun Next's manual [6].

The lane-changing model is a decision model that tries to imitate a real driving behaviour, so some representative questions in order for the driver to make a decision follow:

- *Is it necessary to change lanes?* This depends on factors like the distance to the next turn and the traffic conditions in the current lane.
- *Is it desirable to change lanes?* This is contingent on whether the lane change will result in any improvement in the driver's traffic conditions. This improvement is calculated using speed and distance measures.
- *Is it possible to change lanes?* This depends on whether there is a sufficient gap to perform a lane change. If both the braking imposed by the future downstream vehicle to the vehicle which is considering to change lane and the braking imposed by the vehicle which is considering to change lane to the future upstream vehicle are acceptable, then the lane changing is possible.

Three distinct zones are taken into account to depict the driver's conduct in the lane-changing decision-making process, each of which corresponds to a particular lane-changing motivation.

- *Zone 1*: The decision to change lane is mostly influenced by the traffic conditions in the involved lanes. As a measure of improvement on the driver's traffic conditions, parameters like the desired speed of the driver, the speed and distance of the current preceding vehicle and of the future preceding vehicle in the destination lane are used.
- *Zone 2*: This is the intermediate zone. In this zone, vehicles are driving in lanes, where the desired turn movement cannot be made, so the ones that are looking for a gap adapt their speed in order to target it, whether it is either adjacent to them, or downstream.
- *Zone 3*: Vehicles are in the need to change lane, so they are decreasing their speed, even to zero, in order to find a gap that meets the lane-changing criteria there.

Gap Acceptance Model for Lane Changing

The gap is acceptable if, at time t, the following inequalities hold for both the upstream and downstream gaps:

$$\begin{aligned}\text{Gap}_{Up}(t) \geq \max\Bigg\{ & 0, \frac{V_k^2(t)}{2b_k} + 0.5V_{Up}(t)T_{Up} \\ & + \max\left[0, \left(-\frac{V_{Up}^2(t)}{2b_{Up}} + a_{Up}(1-0.5a_{Up})b_{Up}T_{Up}^2 + (1-a_{Up})V_{Up}(t)T_{Up}\right)\right]\Bigg\}\end{aligned} \tag{3.13}$$

and

$$\begin{aligned}\text{Gap}_{Dw}(t) \geq \max\Bigg\{ & 0, \frac{V_{Dw}^2(t)}{2b_{Dw}} + 0.5V_k(t)T_k \\ & + \max\left[0, \left(-\frac{V_k^2(t)}{2b_k} + a_{Dw}(1-0.5a_{Dw})b_kT_k^2 + (1-a_{Dw})V_k(t)T_k\right)\right]\Bigg\}\end{aligned} \tag{3.14}$$

where ab_k is the maximum desired deceleration and b_k is the estimated desired deceleration of the leader.

Also, the *Lane Changing Cooperation* factor plays a crucial role in the cooperation of vehicles from the left lanes with the requesting-to-turn vehicles in their corresponding right lanes.

HEURISTIC RULES ON LANE-CHANGING MODEL

In general, when entering a drop lane from an on-ramp, at some point vehicles will need to change lane. So, the Gipps lane-changing model (default) is used in all of the network's sections, except for the merging sections, where it shows non-realistic behaviour. In these sections, the Gipps lane-changing model has been replaced within the microSDK by some heuristic rules, developed in [10], in order to achieve a realistic merging behaviour. The heuristic rules are composed of three inequalities, which can be represented by three linear functions relative to the position of a vehicle. Two out of three inequalities ensure that a vehicle's current speed and available gap in the target lane are greater than some - relative to its position in the section - lower bound. The third inequality checks if the speed difference of a vehicle's speed, with respect to the speed of the vehicle upstream on the target-lane, if any, is less than some - relative to it's position in the section - upper bound. If this set of inequalities holds for a vehicle, then it is mandated to make a turn to the target-lane. As seen in Figure 3.2, while a vehicle is moving downstream, these three thresholds become more relaxed, until the vehicle reaches some defined positions in the section and each of these functions becomes constant for the rest of it. In order to determine these rules, the required parameters are the slope, the initial and the final values of the linear equations [10].

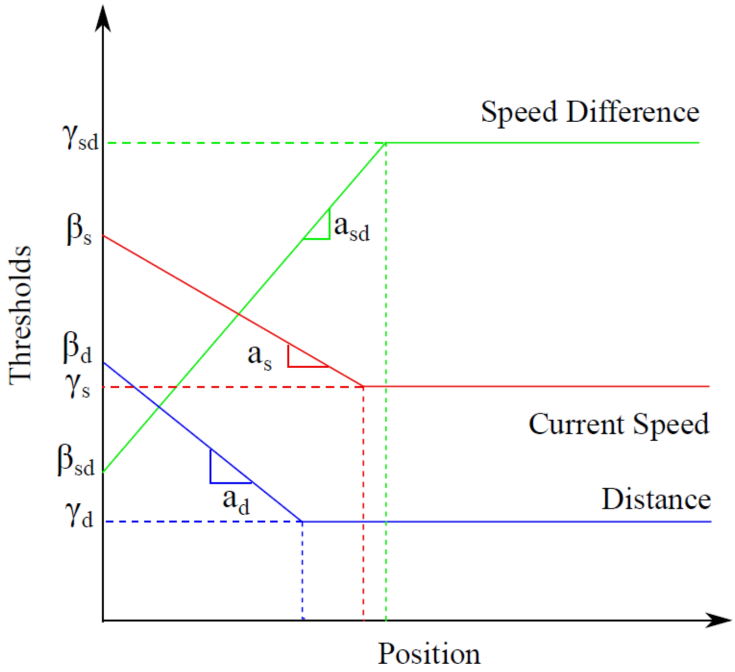

FIGURE 3.2: Heuristics replacing the default lane-changing model

3.3 REAL-TIME ACC-BASED TRAFFIC CONTROL ADAPTATION STRATEGY

ACC-vehicles can be employed as actuators in mixed traffic situations to improve traffic flow efficiency. Drivers of ACC-vehicles are often supplied a range, e.g. of $0.8 - 2.2$ *sec* [13], to select their desired time-gap to the front vehicle. The default or maximum time-gap value in ACC-equipped vehicles is frequently in the range of $1.8 - 2.2$ *sec*, even though drivers may select the ACC settings from a provided range [5]. The time-gap of ACC-vehicles could be changed dynamically in real time through a control strategy, in the purpose of boosting the motorway capacity. The control strategy presented in this thesis depends only on real-time measurements of flow and mean speed. It is activated only when, where and to the extent needed.

Consider a motorway with both manually-driven and ACC-vehicles. The ACC-vehicle drivers may insert their desired ACC system settings, i.e. desired speed v_d and time-gap T_d, but these settings may change, if the control strategy suggests different values. This motorway is divided into sections and the traffic management centre (or road-side unit, RSU) applies this strategy at every section independently. At every control interval, the RSU receives the exiting flow q_i of each section i (or an estimate of it, like in the previous chapter) and its mean speed v_i (via V2I communication or spot-sensors). It then decides, in real-time, the suitable ACC settings for each section and it communicates them via V2I communication.

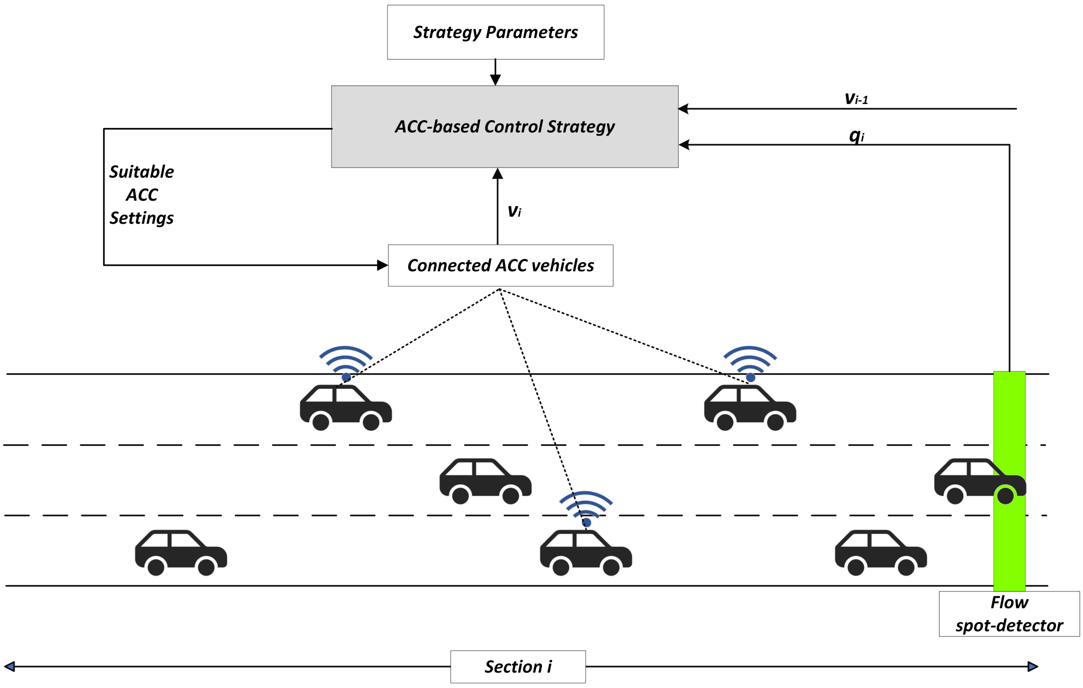
Strategy Parameters
ACC-based Control Strategy
v_{i-1}
q_i
Suitable ACC Settings
v_i
Connected ACC vehicles
Flow spot-detector
Section i

FIGURE 3.3: Illustration of the control strategy in action

This strategy aims at two goals: capacity increase and discharge flow increase. The relative theory below has been developed in [5].

3.3.1 CAPACITY INCREASE

The strategy gradually decreases the suggested time-gap as a function of traffic flow $T_i[q_i(k)]$ for section i, like in Figure 3.4. So, for flow values lower than Q_1, it suggests T_{max}, because traffic is undercritical, and for flow values greater than Q_1 and less than or equal to Q_2, the suggested value is being gradually decreased, until it reaches T_{min}. If traffic flow exceeds an upper bound Q_2, which is less than capacity Q_{cap}, the strategy suggests T_{min} in order to avert a congestion getting formed. This means that this section's capacity is going to increase, reaching the maximum.

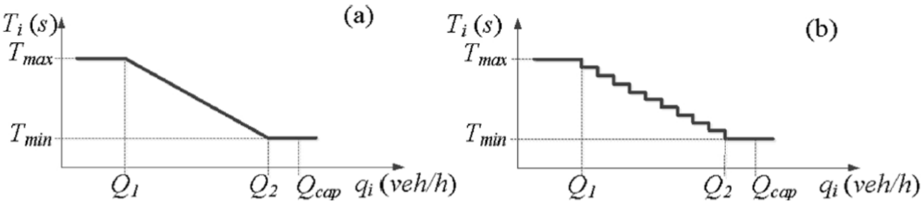

FIGURE 3.4: Time-gap strategy using: (a) a linear, or (b) a stepwise function [5]

But if, even after the capacity increase, congestion is formed, meaning that the section's average velocity $v_i(k)$ becomes smaller than some predefined speed lower bound V_{cong}, then in an effort to open up the gaps between congested vehicles, so they can increase their speed and make a turn to another lane, and for safety reasons, the strategy suggests T_{max}.

So, the strategy decides to suggest a time-gap value based on the following formula:

$$T_{stg,i} = \begin{cases} T_i[q_i(k)], & \text{if } \mathrm{v}_i(k) > V_{cong} \\ T_{max}, & \text{else} \end{cases} \tag{3.15}$$

It should be noted, that V_{cong} can be inferred from historical data.

3.3.2 DISCHARGE FLOW INCREASE

According to [5], it is empirically known that the discharge flow at the area of the congestion head is lower than capacity, so the goal is to dynamically reduce this capacity drop and increase the discharge flow at active bottleneck locations.

The strategy locates congestion heads. Locating a congestion head can be done by observing two consecutive sections and realizing that the first one $(i-1)$ upstream of the bottleneck has a mean speed $\mathrm{v}_{i-1}(k)$ less than V_{cong} and the second one (i) downstream of the bottleneck $\mathrm{v}_i(k)$ greater than V_{cong}, while the subtraction of their speeds $\mathrm{v}_i(k) - \mathrm{v}_{i-1}(k)$ is greater than a predefined threshold $\Delta\mathrm{v}$; e.g. $\Delta\mathrm{v} = 10$ km/h.

Once a congestion head is found, the suggested time-gap of only these two sections becomes T_{min}. This decision is on top of the aforementioned decisions in 3.15. This means that, if this triple condition holds, these are the actions that the controller will suggest, else the decisions in 3.15 will be suggested.
The conditions and the actions follow:

$$\begin{aligned} &\text{if } \mathrm{v}_i(k) > V_{cong} \text{ and } \mathrm{v}_{i-1}(k) < V_{cong} \text{ and } [\mathrm{v}_i(k) - \mathrm{v}_{i-1}(k)] > \Delta\mathrm{v} \\ &T_{stg,i}(k) = T_{min} \text{ and } T_{stg,i-1}(k) = T_{min} \end{aligned} \tag{3.16}$$

Finally, the time-gaps suggested by the controller are applied according to the relation:

$$T_{applied,j} = \min\{T_{d,j}, T_{stg,i}\} \tag{3.17}$$

with $T_{d,j}$ being the initial, individual time-gap given by the predefined time-gap normal distribution to ACC-vehicle j.

It should be noted that these values and these decisions are momentary, so it would not be desired for them to be applied in a stop-and-go wave situation. So, in order to determine that a bottleneck is stationary, persistency tests should also be included [5].

3.4 NETWORK

A toy network (Figure 3.5) was created in order to demonstrate the effectiveness of the control strategy. The network consists of 10 sections, arranged in a straight road, and an on-ramp at the end of section 7. Every section contains its own spot-sensor at the end of it, like in Figure 3.3. All sections contain two lanes, except for the eighth, which consists of three lanes; two coming from the previous section and the acceleration lane for the vehicles that come from the on-ramp. The traffic flow direction is from the first section to the tenth.

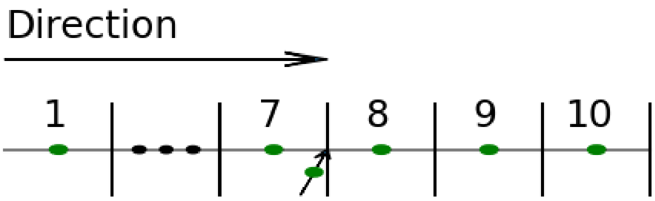

FIGURE 3.5: The toy network developed in the Aimsun Next tool for testing the two ACC control adaptation scenarios

The characteristics of the active bottleneck of the congestion formed in the 8th section are depicted in the Figures 3.6 and 3.7. As it can be seen from these Figures, mild congestion begins to form from the 20th minute and then strong congestion is formed between the 30th and the 50th minute. More specifically, it is observed in these two Figures that, between the 20th and the 30th minute, traffic flow is concentrated around 4400-4500 veh/h, and at the 30th minute, there is a drop in traffic speed and flow (traffic flow breakdown). Afterwards, from the 30th to the 50th minute, traffic flow lies around 4000 veh/h, while the density subfigure of 3.7 shows that the whole section is getting full (it is full between the 40th and the 50th minute) of congested vehicles. Also, the speed subfigure shows that the drivers are experiencing lower speeds. So the capacity drop is around 8.5-11%. Utilizing the relation $q = \rho v$ and these data, it is verified that the combination of high densities and low speeds produce low flows [14]. The spillback of the congestion reaches up to 400-500m upstream of the bottleneck location. After the 50th minute, free-flow conditions prevail again.

We would have used the Antwerp network from the previous chapter, instead of a toy network, but the current stretch did not produce the appropriate congestion, as it was not created due to active bottlenecks. This can also be deduced from the scattered, not concentrated data points at high density values in Figure 2.13.

3.5 SIMULATION PARAMETER SETUP

The simulation parameters that played a crucial role in achieving a congestion with the models used, follow.

For the car following model, the minimum headway was decided for each vehicle by a normal distribution with values inside the interval $[1.0\,sec,\ 1.6\,sec]$

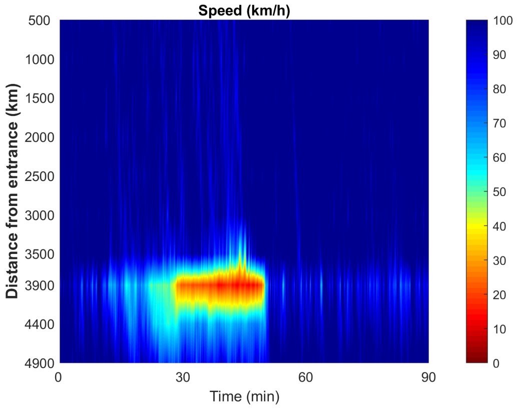

FIGURE 3.6: Speed contour plot of the toy network

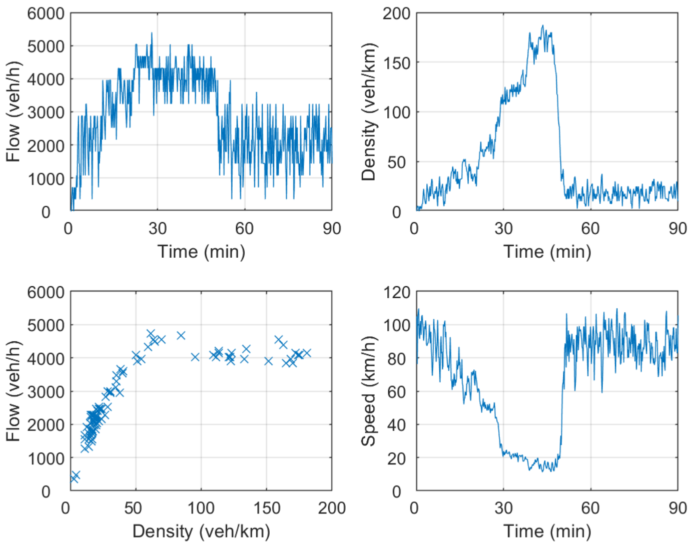

FIGURE 3.7: Traffic flow, density, fundamental diagram and speed of section 8

with mean value $\mu = 1.3\ sec$ and standard deviation $\sigma = 0.05\ sec$. The sensitivity factor for conventional vehicles was set to 1.08, 2, 1.5 and 1.2 for sections 1-7, 8, 9 and 10, respectively. Also, for the ACC-vehicles, the sensitivity factor was set to 1.08 for all sections and the speed gain free-flow k_1, the speed gain following k_3 and the distance gain k_2 from 3.2.1 were set to 0.8 sec^{-1}, 0.8 sec^{-1} and 0.023 sec^{-2}, respectively. Finally, the initial desired time-gaps of Aimsun's default ACC-vehicles were chosen by a normal distribution with values within the interval $[0.8\ sec,\ 2.2\ sec]$, with mean $\mu = 1.8\ sec$ and standard deviation $\sigma = 0.25\ sec$.

The Gipps car-following model is described by many researchers as inadequate for modeling a congestion that approaches reality. For instance, Wang et al. [15], [16] commented that the Gipps model was unable to reproduce traffic breakdown and hysteresis. Ciuffo et al. [17] pointed out that the Gipps model includes some coefficients that are hard to interpret for their physical meaning.

Nevertheless, handling the Sensitivity Factor α using logic through the API programming-environment, it was discovered that a small congestion can be formed (see Figure 3.6), without abnormal driving behaviors.

With a sensitivity factor close to 1, cars go very fast and not only congestion cannot be formed, but also the driving behavior is unrealistic, as it cannot reproduce traffic breakdown and hysteresis at the bottleneck location. On the other side, an α greater than 2-2.5 produces slow speeds, when they should be free-flow speeds, also making the scenario unrealistic. All sensitivity factor characteristic combinations were tested via the trial and error method (< 1, > 1, $= 1$) before, in and after section 8. The only one that produced an acceptable result was the one which had a sensitivity factor α close to 1 before section 8, α close to 2 in section 8 and then gradually getting lowered close to 1 again. Specifically in sections 1 to 7, 8, 9 and 10, α was set to 1.08, 2, 1.5 and 1.2, respectively. Note that this applies only to vehicles without the ACC capability. This is because vehicles with ACC are already "cautious" in keeping distance to their leader in order to keep their time-gap, whether they perform control adaptation or not. The α factor for ACC-vehicles is 1.08.

For the lane-changing model, the default model was kept for all sections [9] apart from the 8^{th} section, in which the heuristic rules described in Figures 3.8 and 3.9 override the default one.

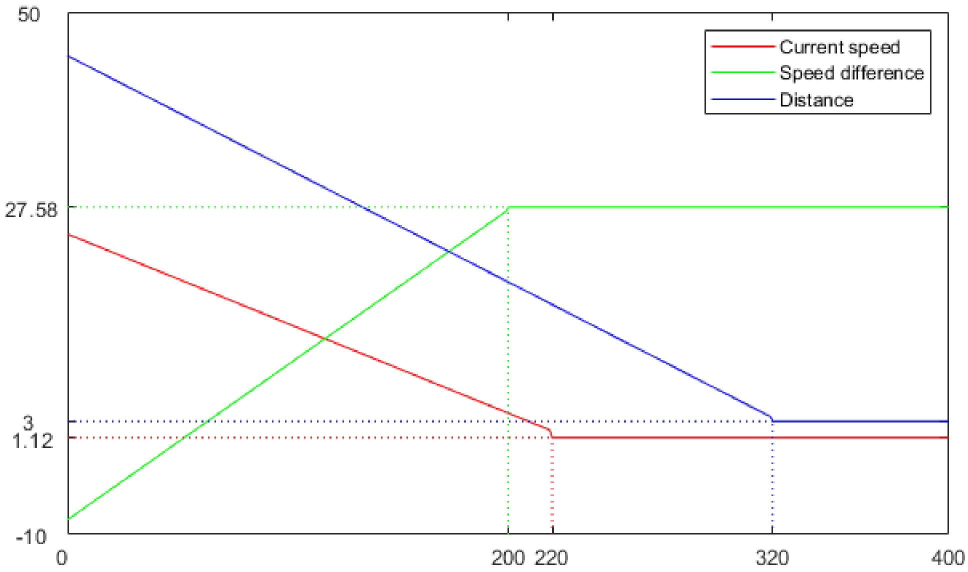

FIGURE 3.8: Heuristic lane-changing rules applied in the acceleration lane of section 8 in the toy network

For the controller, the stepwise function was preferred and $V_{cong} = 60$ km/h, $Q_1 = 1350$ veh/h, $Q_2 = 1900$ veh/h, the ACC Steps were set to 14, $\Delta v = 10$ km/h, $T_{min} = 0.8$ *sec*, $T_{max} = 2.2$ *sec*, the Area Control Time was set to 30 *sec* and the Area Measurement Interval was 10 *sec*.

The parameters describing the acceleration lane in section 8 were the *side lane cooperation distance*, the *side lane merging distance* and the *side lane merge*.

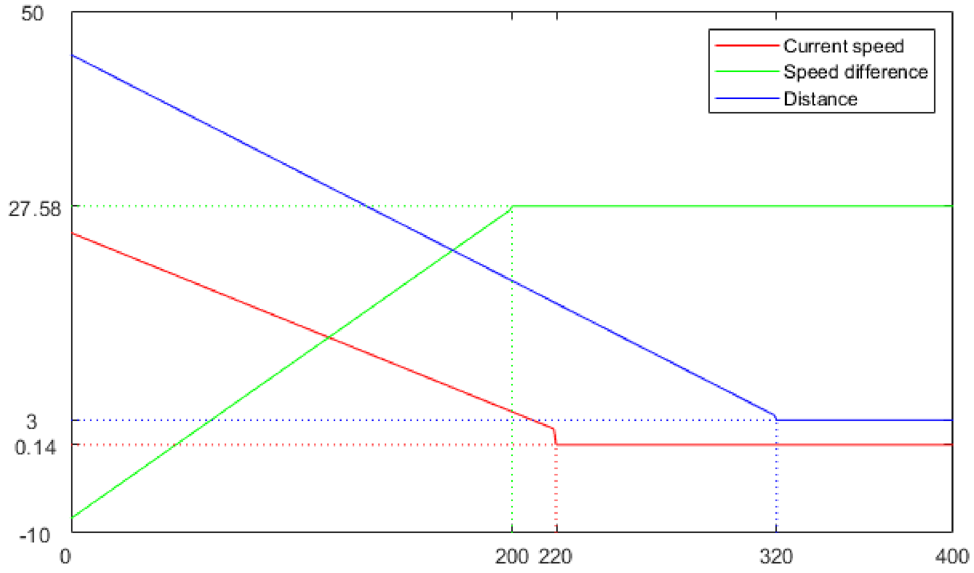

FIGURE 3.9: Heuristic lane-changing rules applied in the middle lane of section 8 in the toy network

Side lane cooperation distance is the distance from the ramp's end, at which a vehicle can begin to expect cooperation from other vehicles on the main lanes in order to change lane. It was set to 30m. *Side lane merging distance* is the distance from the ramp's end, where vehicles begin to merge into the main lanes. It was set to 20m. *Side lane merge* was set to FIFO. This is outgeneraled by the heuristic lane-changing rules applied in the acceleration lane, but absolutely needed for making the driving behavior acceptable during congestion.

Last, but not least, both the simulation step and the reaction time were set equal to 0.1 *sec* [6].

3.6 EXPERIMENTAL RESULTS

The experimental results will be presented with the following order: No ACC Control Adaptation case, ACC Control Adaptation scenario 1 (3.3.1), ACC Control Adaptation scenario 2 (3.3.2). Ten replications of the experiment were run for each case/scenario and for each penetration rate to account for the stochasticity in the experiments and derive safer results. The penetration rate PR is the percentage of the ACC-vehicles in the network.

3.6.1 NO ACC CONTROL ADAPTATION

In this case, each ACC-vehicle chooses a desired time-gap between 0.8 *sec* and 2.2 *sec*, with $\mu = 1.8$ *sec* and $\sigma = 0.25$ *sec*. No strategy is employed.

The heatplots in 3.10 are extracted from the replication closest to the average for penetration rates 0%, 50% and 100%. The average case is described by the averaged TTS (Total Time Spent in the network) and AVD (Average

Vehicle Delay) measurements of all ten replications that have been run, as is usual in experimental, statistical procedures. In the current scenario, the default values of Aimsun's ACC controller are employed.

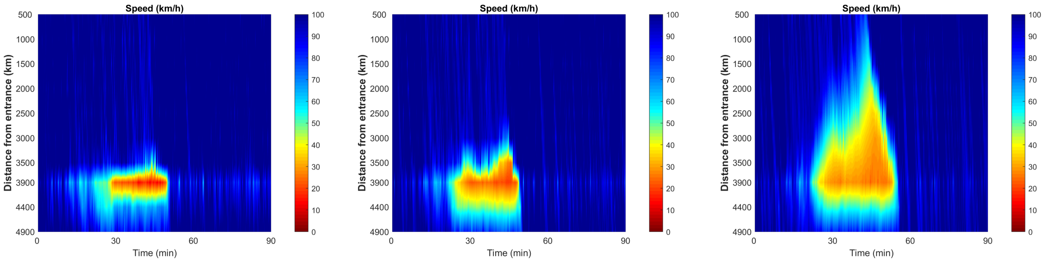

PR 0% PR 50% PR 100%

FIGURE 3.10: No ACC Control Adaptation case for PR 0%, 50% and 100%

PR	TTS($veh \times h$)	Difference(%)	AVD($sec/veh/km$)	Difference(%)
0%	200.708	-	14.8761	-
10%	203.151	1.22	15.7566	5.92
20%	196.334	-2.18	12.7454	-14.32
30%	197.153	-1.77	12.8662	-13.51
40%	203.238	1.26	14.7375	-0.93
50%	208.343	3.80	16.1541	8.59
60%	213.253	6.25	17.3198	16.43
70%	216.303	7.77	17.7409	19.26
80%	221.354	10.29	18.6013	25.04
90%	225.298	12.25	19.1419	28.68
100%	231.537	15.36	20.0606	34.85

TABLE 3.1: No ACC Control Adaptation case: Total Time Spent (TTS) and Average Vehicle Delay (AVD) considering various PR

As referenced above, Wang et al. commented that the Gipps model is unable to reproduce traffic breakdown and hysteresis. So, the combination of the Gipps lane-changing heuristic and the sensitivity factor $\alpha = 2$ in section 8 produces an austere model. So, even with no ACC control adaptation, at slower speeds vehicles that have the ACC ability leave larger time-gaps with their leaders, thus creating larger space-gaps allowing vehicles from the lane to their right to take a left turn. That is why in higher penetration rates, speeds are not totally as low as the 0% case and that is also why, representatively, in Table 3.1 the 20%'s TTS and AVD difference with the 0% case is negative. But, as the penetration rate grows, not performing control adaptation, constantly, almost linearly increases the TTS and AVD time metrics greatly, as seen in Figures 3.11, 3.12 and Table 3.1 and in the heatplots 3.10.

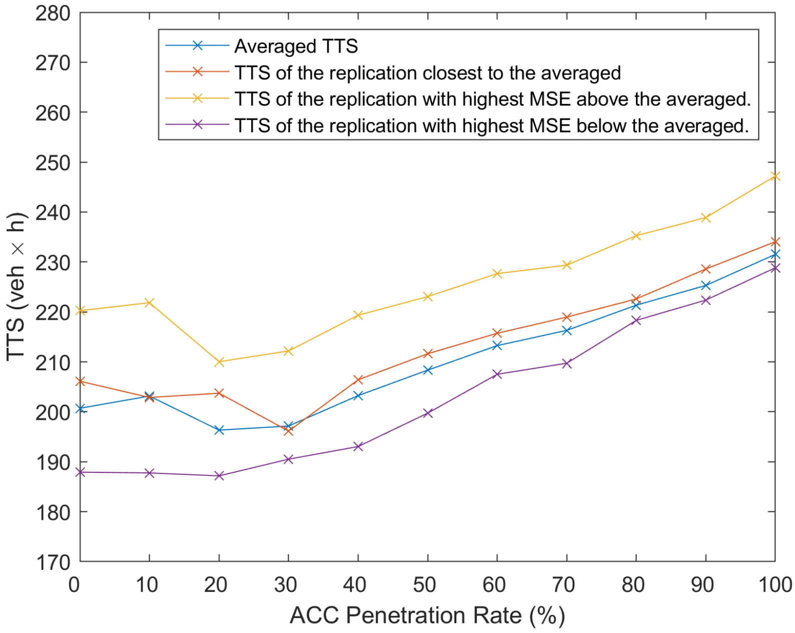

FIGURE 3.11: No ACC Control Adaptation case: Total Time Spent (TTS) considering various PR

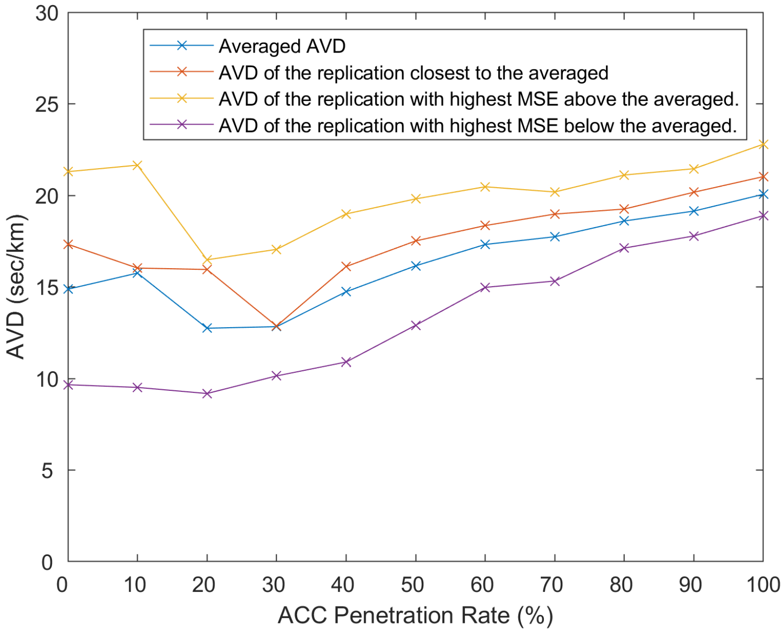

FIGURE 3.12: No ACC Control Adaptation case: Average Vehicle Delay (AVD) considering various PR

And of course, the no ACC control adaptation case is never close to the control adaptation scenarios 1 and 2, as it will be shown later below.

Clarifying, Figures 3.11 and 3.12, and the corresponding Figures later below, contain four graphs. From these, only the averaged TTS/AVD is not a replication. Instead, it is an average of all ten replications for each penetration rate. The other three are specific replications, that were chosen to be plotted with the use of the Mean Square Error criterion. The replications with the highest MSE above and below the averaged are shown as replications-limits, while the replication closest to the averaged is the one with the smallest MSE. All MSE values were calculated with respect to the averaged TTS/AVD.

Finally, Table 3.1 lists the TTS and AVD values over each penetration rate, as seen in Figures 3.11, 3.12, and, also, reports the percentage difference of each penetration rate with the PR=0% case.

3.6.2 ACC Control Adaptation scenario 1

In this case, the first part (equation 3.15) of the proposed traffic control concept is employed. Like in the previous case, the heatplots in 3.13 are extracted from the replication closest to the average, this time for penetration rates 20%, 50% and 100%. It is clear from Figures 3.14, 3.15 and Table 3.2 that the TTS and AVD metrics are significantly decreasing, as the PR increases and that the congestion is getting remarkably reduced.

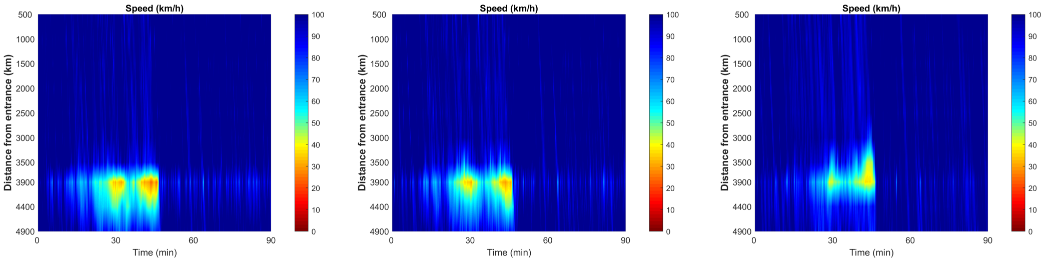

PR 20% PR 50% PR 100%

FIGURE 3.13: ACC Control Adaptation scenario 1 for PR 20%, 50% and 100%

	TTS$(veh \times h)$			AVD$(sec/veh/km)$		
PR	No Control	Control Case 1	Improvement(%)	No Control	Control Case 1	Improvement(%)
0%	200.708	-	-	14.8761	-	-
10%	203.151	197.617	2.72	15.7566	13.6122	13.61
20%	196.334	190.305	3.07	12.7454	10.7216	15.88
30%	197.153	190.431	3.41	12.8662	10.6986	16.85
40%	203.238	190.075	6.48	14.7375	10.5452	28.45
50%	208.343	189.272	9.15	16.1541	10.252	36.54
60%	213.253	185.378	13.07	17.3198	9.04235	47.79
70%	216.303	185.195	14.38	17.7409	8.9868	49.34
80%	221.354	183.922	16.91	18.6013	8.56363	53.96
90%	225.298	183.002	18.77	19.1419	8.24538	56.92
100%	231.537	180.854	21.89	20.0606	7.57313	62.25

TABLE 3.2: ACC Control Adaptation scenario 1: Total Time Spent (TTS) and Average Vehicle Delay (AVD) considering various PR

Table 3.2 lists the no ACC control adaptation and ACC control adaptation scenario 1 values over all penetration rates, and for each PR, the percentage improvement.

It should be taken into consideration that due to the formula $T_{applied,j} = min\{T_{d,j}, T_{stg,i}\}$, to the fact that the maximum time-gap suggested by the controller is selected to be $T_{max} = 2.2\ sec$ and to the fact that the normal distribution of the initial desired time-gap is chosen to be in the interval $[0.8\ sec, 2.2\ sec]$ with $\mu = 1.8\ sec$ and $\sigma = 0.25\ sec$, the adopted desired time-gap, when in congestion ($\mathrm{v}_i(k) < V_{cong}$), is equal to $T_{max} = 2.2\ sec$, only when $T_{d,j} = T_{max} = 2.2\ sec$.

To give an example of the time-gap suggestions made by the controller, Figure 3.16 depicts the flow, density, the time-gap suggested by the control

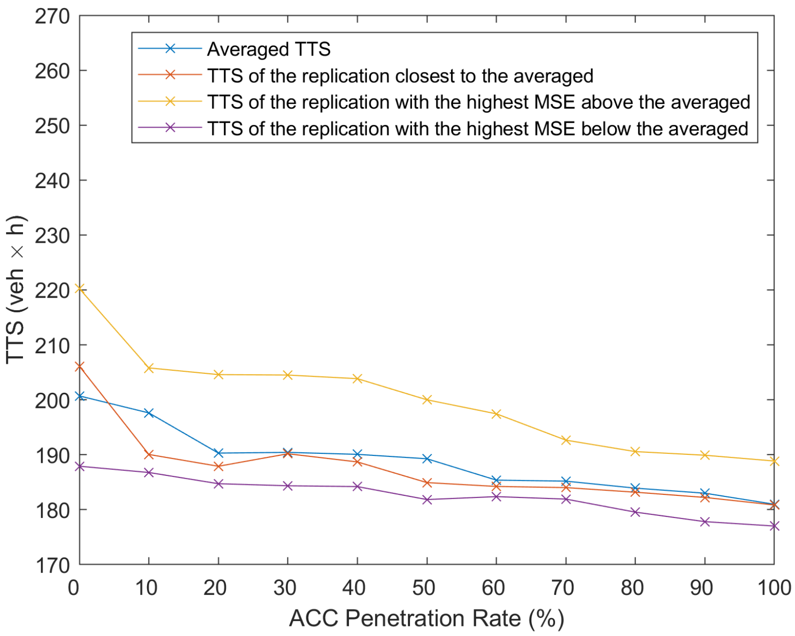

FIGURE 3.14: ACC Control Adaptation scenario 1: Total Time Spent (TTS) considering various PR

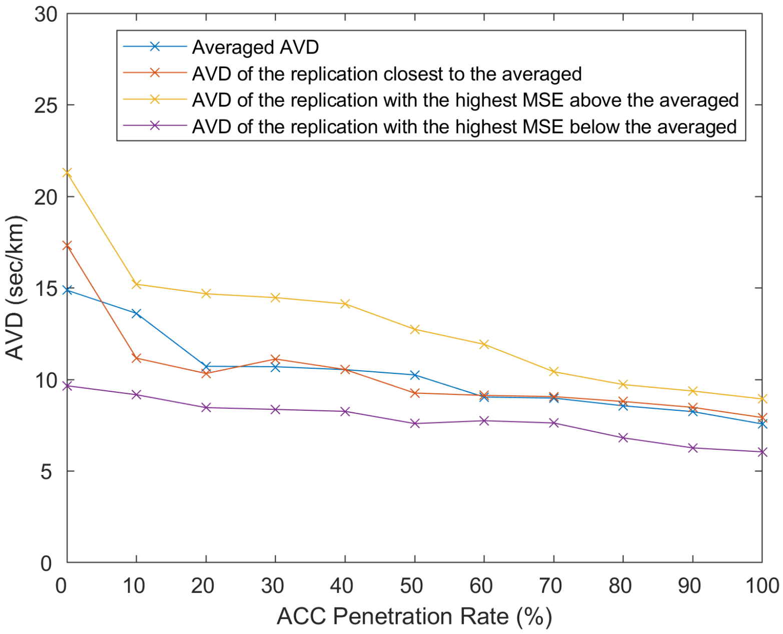

FIGURE 3.15: ACC Control Adaptation scenario 1: Average Vehicle Delay (AVD) considering various PR

strategy and speed at section 8 for a penetration rate equal to 30%. It is observed that, as long as the speed is below $V_{cong} = 60$ km/h, meaning that congestion starts to form or has already formed, the strategy suggests a time-gap equal to $T_{max} = 2.2$ *sec*, in order to open up the gaps between the vehicles. Otherwise, the time-gap is decided based upon the section's flow, according to the stepwise function in Figure 3.4, within 14 steps. Note that, for flows close to $\#lanes \times Q_2 = 2 \times 1900\frac{veh}{h} = 3800\frac{veh}{h}$ and speeds greater than $V_{cong} = 60$ km/h, like the ones around the 20^{th} minute, the strategy suggests small time-gaps, trying to increase the section's capacity and avoid the formation of congestion. It is evident that the flow is, in general, higher (around 4400 veh/h) than the flow, when in congestion, in the case of PR=0% (see Figure 3.7), greatly mitigating the capacity drop phenomenon, and that the drivers are experiencing higher speeds than the ones in the PR 0% case.

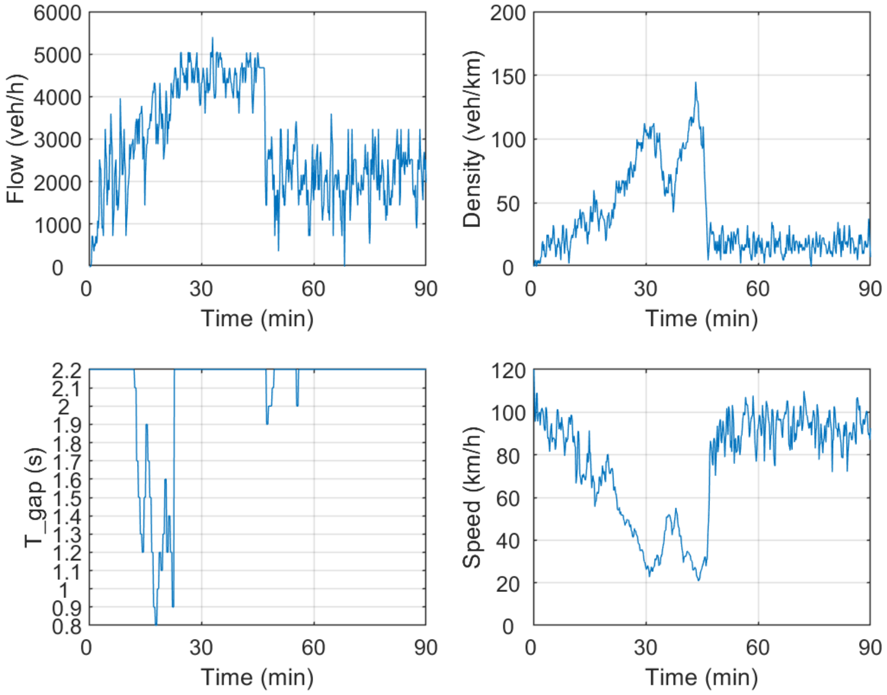

FIGURE 3.16: ACC Control Adaptation scenario 1: Flow, density, ACC time-gap suggestions made by the strategy and speed at section 8 for PR=30%

3.6.3 ACC CONTROL ADAPTATION SCENARIO 2

In this case, the equations of scenario 2 (3.16) of the proposed traffic control concept are employed on top of the first scenario's equation (3.15). Like in the previous cases, the heatplots in 3.17 are extracted from the replication closest to the average for the penetration rates of 20%, 50% and 100%. It is clear from Figures 3.18, 3.19 and Table 3.3 that the TTS and AVD metrics are remarkably decreasing as the PR increases and the congestion is getting even more reduced than in the previous case.

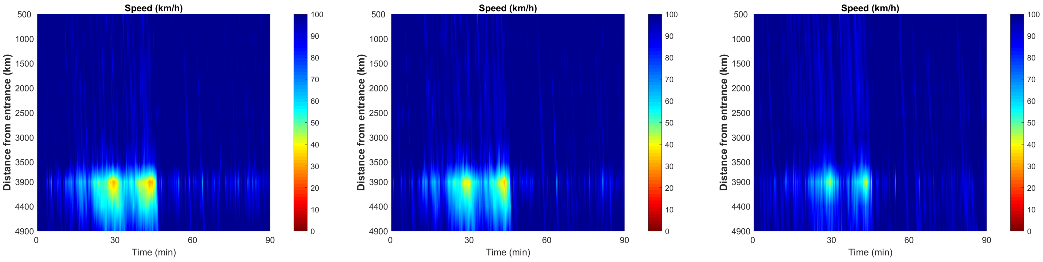

PR 20% PR 50% PR 100%

FIGURE 3.17: ACC Control Adaptation scenario 2 for PR 20%, 50% and 100%

PR	TTS($veh \times h$)			AVD($sec/veh/km$)		
	No Control	Control Case 2	Improvement(%)	No Control	Control Case 2	Improvement(%)
0%	200.708	-	-	14.8761	-	-
10%	203.151	195.432	3.8	15.7566	12.863	18.36
20%	196.334	189.918	3.27	12.7454	10.8037	15.23
30%	197.153	185.501	5.91	12.8662	9.09563	29.31
40%	203.238	185.993	8.49	14.7375	9.34871	36.57
50%	208.343	183.301	12.02	16.1541	8.36545	48.21
60%	213.253	181.475	14.9	17.3198	7.80668	54.93
70%	216.303	180.365	16.61	17.7409	7.43225	58.11
80%	221.354	179.308	18.99	18.6013	7.08006	61.94
90%	225.298	177.867	21.05	19.1419	6.63859	65.32
100%	231.537	176.915	23.59	20.0606	6.32809	68.46

TABLE 3.3: ACC Control Adaptation scenario 2: Total Time Spent (TTS) and Average Vehicle Delay (AVD) considering various PR

Table 3.3 lists the no ACC control adaptation and ACC control adaptation scenario 2 values over all penetration rates, and for each PR, the percentage improvement compared to the one without control adaptation.

Like at the end of the previous scenario, an example of the time-gap suggestions made by the control strategy are displayed in Figures 3.20 and 3.21. In these Figures there are the flow, density, the time-gap suggested by the strategy and speed at sections 8 and 9 for a penetration rate equal to 30%. It is reminded that, in this scenario, equation 3.16 is used on top of 3.15.

Figure 3.20 shows the effect of both equations on section 8. Until the last time that the time-gap is equal to 0.9 sec before the 30^{th} minute, the decisions

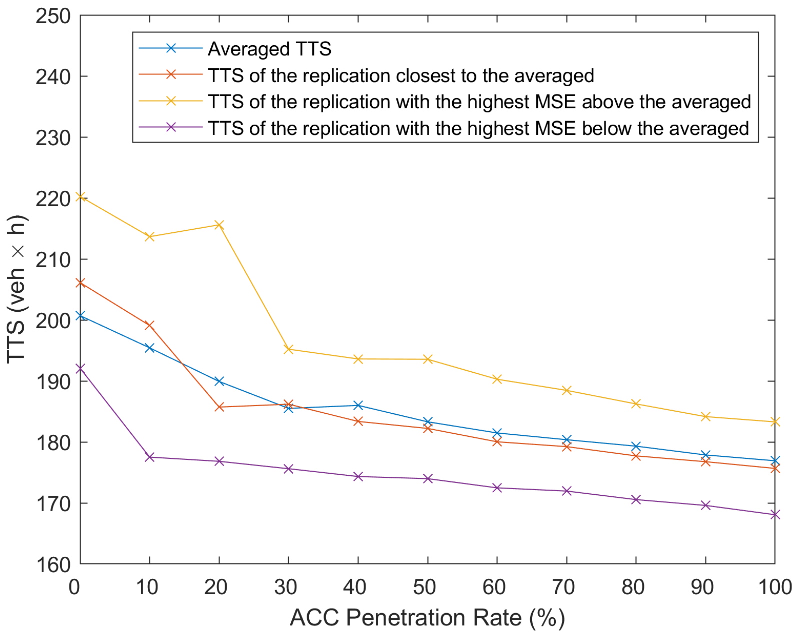

FIGURE 3.18: ACC Control Adaptation scenario 2: Total Time Spent (TTS) considering various PR

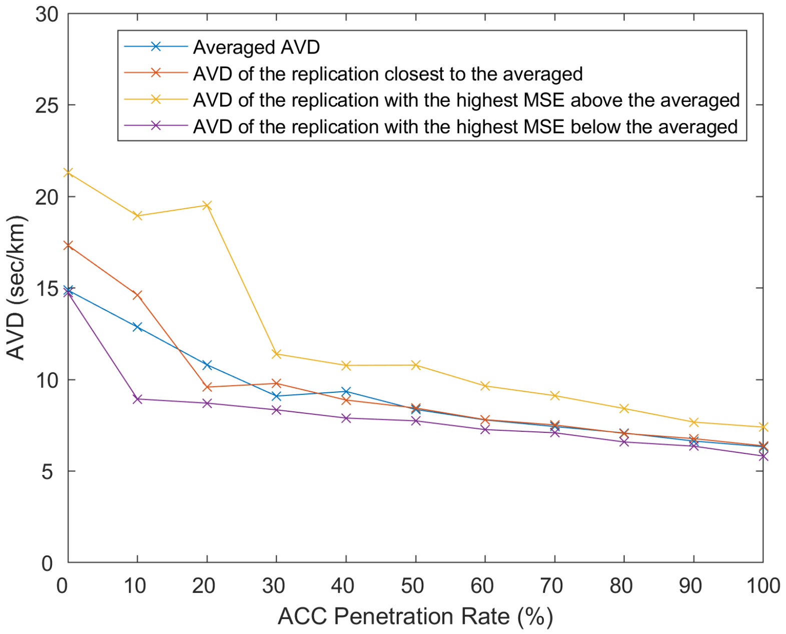

FIGURE 3.19: ACC Control Adaptation scenario 2: Average Vehicle Delay (AVD) considering various PR

are the same with the previous scenario's decisions (see Figure 3.16). In the previous scenario, the next decision was 2.2 *sec*. But now, the conditions of equation 3.16 hold, so the decision is $T_{min} = 0.8$ *sec*, in an attempt to increase the discharge flow. But after this, congestion still manages to form. So, the time-gap decision is $T_{max} = 2.2$ *sec*, because either v₉, that is, the mean speed of section 9, is lower than or equal to $V_{cong} = 60$ km/h, or Δv is less than or equal to 10 km/h. So, the equation in effect switches to 3.15, because the conditions in equation 3.16 are not satisfied. So, equation 3.15 suggests T_{max}, because $v_8 \leq V_{cong}$ in that time interval (v_8 is the mean speed of section 8). Afterwards, once again, in an attempt to increase the discharge flow, the time-gap decision toggles between 0.8 *sec* and 2.2 *sec*. This happens around the 35^{th} minute and around the 40^{th}, when both v_8 and v_9 are very close to V_{cong}, while their flows are greater than $2 \times Q_2 = 2 \times 1900\frac{veh}{h} = 3800\frac{veh}{h}$. So, the decision 2.2 *sec* may come from $v_9 \leq V_{cong}$ and $v_8 \leq V_{cong}$, or $\Delta v \leq 10$ km/h and $v_8 \leq V_{cong}$. Also, the decision 0.8 *sec* may come from 3.16, or, when the conditions in 3.16 are not satisfied and $v_8 > V_{cong}$, since the flow in section 8 is greater than or equal to 3800 veh/h during this time interval. Before the 15^{th} and after the 45^{th} minute, the strategy suggests T_{max}, because traffic is undercritical, that is, the flow is less than or equal to $2 \times Q_1 = 2 \times 1350\frac{veh}{h} = 2700\frac{veh}{h}$.

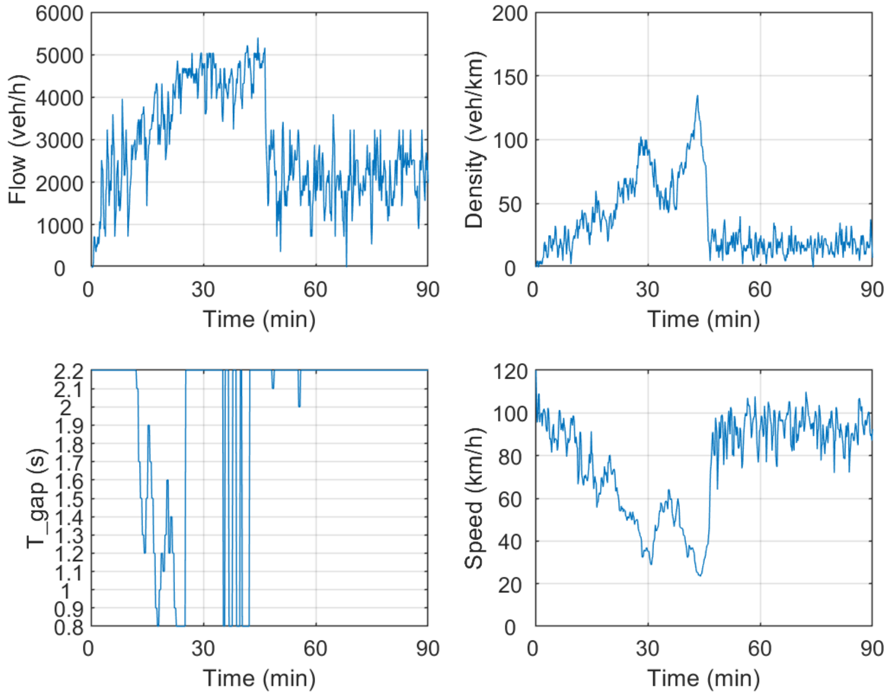

FIGURE 3.20: ACC Control Adaptation scenario 2: Flow, density, ACC time-gap suggestions made by the strategy and speed at section 8 for PR=30%

In section 9 (Figure 3.21), until the 20^{th} minute, the time-gap suggested by the strategy decreases according to the stepwise function in Figure 3.4, as the flow increases, within 14 possible steps. Since the 20^{th} minute, the decision is 0.8 *sec*, either due to equation 3.16, or because the conditions of this equation are not satisfied and the flow is, clearly, greater than 3800 veh/h and $v_9 > V_{cong}$. Also, when the decision is 2.2 *sec*, it is because traffic is undercritical.

Finally, it is evident from the flow subfigure of Figure 3.20, that the flow of section 8 is, in general, greater (around 4400 veh/h) than the flow, when in congestion, in the case of PR=0% (see Figure 3.7), mitigating the capacity drop phenomenon to a great extent, and that the vehicle speeds are higher than the ones in the PR 0% case. Note that, for the ACC penetration rate being 30%, the TTS and AVD measurements are improved by 2.59% and 14.98%, respectively, from the previous scenario, when equation 3.16 was not employed.

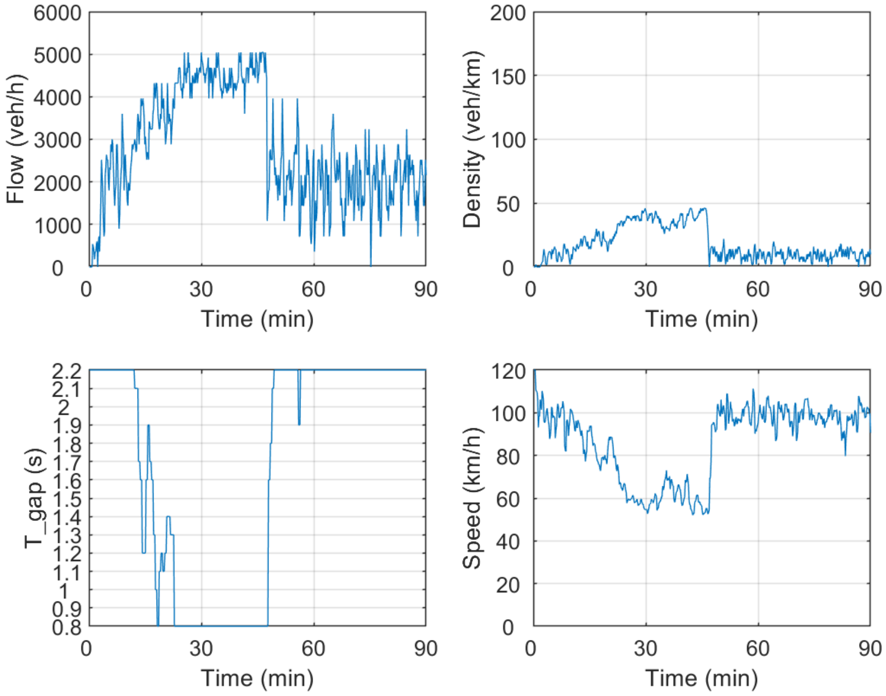

FIGURE 3.21: ACC Control Adaptation scenario 2: Flow, density, ACC time-gap suggestions made by the strategy and speed at section 9 for PR=30%

3.6.4 NO ACC CONTROL ADAPTATION AND ACC CONTROL ADAPTATION SCENARIOS 1 AND 2

The objective of this section is to compare the no control adaptation case, the control adaptation scenario 1 and scenario 2 with each other, utilizing the TTS and AVD metrics. Figures 3.22, 3.23 compare the TTS and AVD metrics for the three cases over all PRs, Table 3.4 shows the percentage difference between scenario 1 and scenario 2 over all PRs and Figures 3.24, 3.25 depict the difference of the TTS, AVD metrics between scenario 1 and the no adaptation case, scenario 2 and the no adaptation case, and scenario 2 and scenario 1.

It is evident from Figures 3.22, 3.23, 3.24, 3.25 and Table 3.4, that the scenario in which equation 3.15 is employed manages to reduce the TTS and AVD compared to the no control adaptation case, and the scenario in which equations 3.16 are employed on top of 3.15 manages to further reduce the TTS and AVD, compared to using only equation 3.15. Considering the difference between the two ACC control adaptation scenarios, the second is more efficient than the first for every penetration rate for the TTS metric, and also for the AVD metric, except for the 20% case (for the AVD) where control scenario 1 is 0.77% better than control scenario 2. This is, understandably, due to the fact that only ten replications were run.

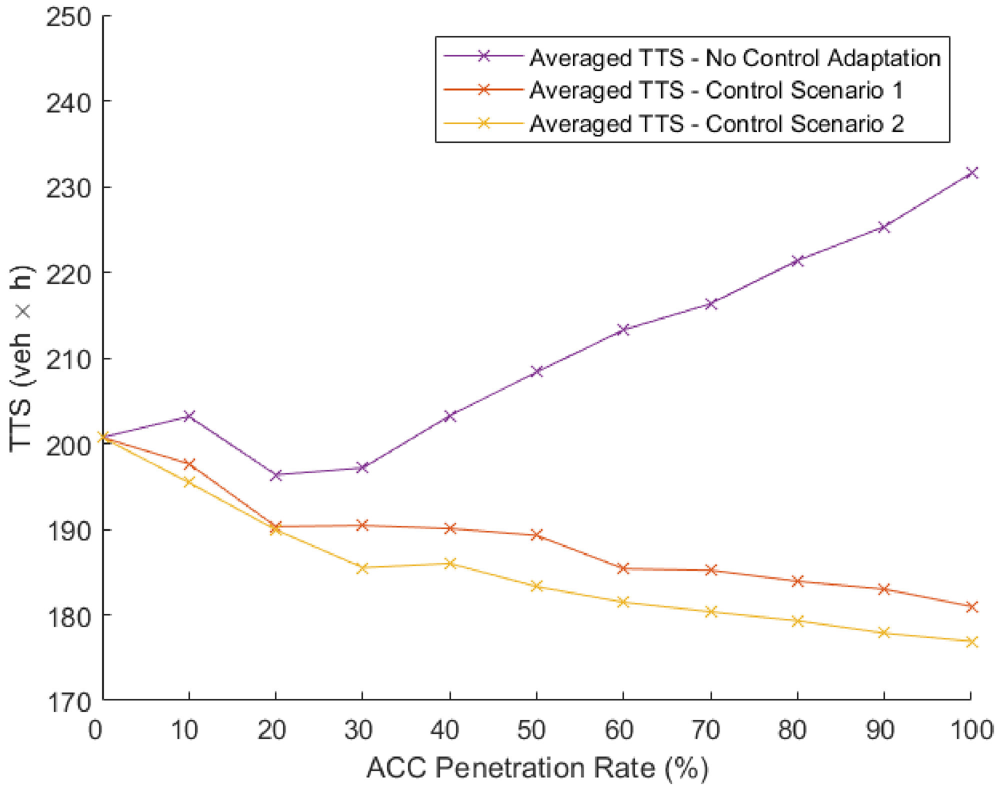

FIGURE 3.22: Comparison of the Total Time Spent (TTS) for the No ACC Control Adaptation case, the ACC Control Adaptation scenarios 1 and 2 considering various PR

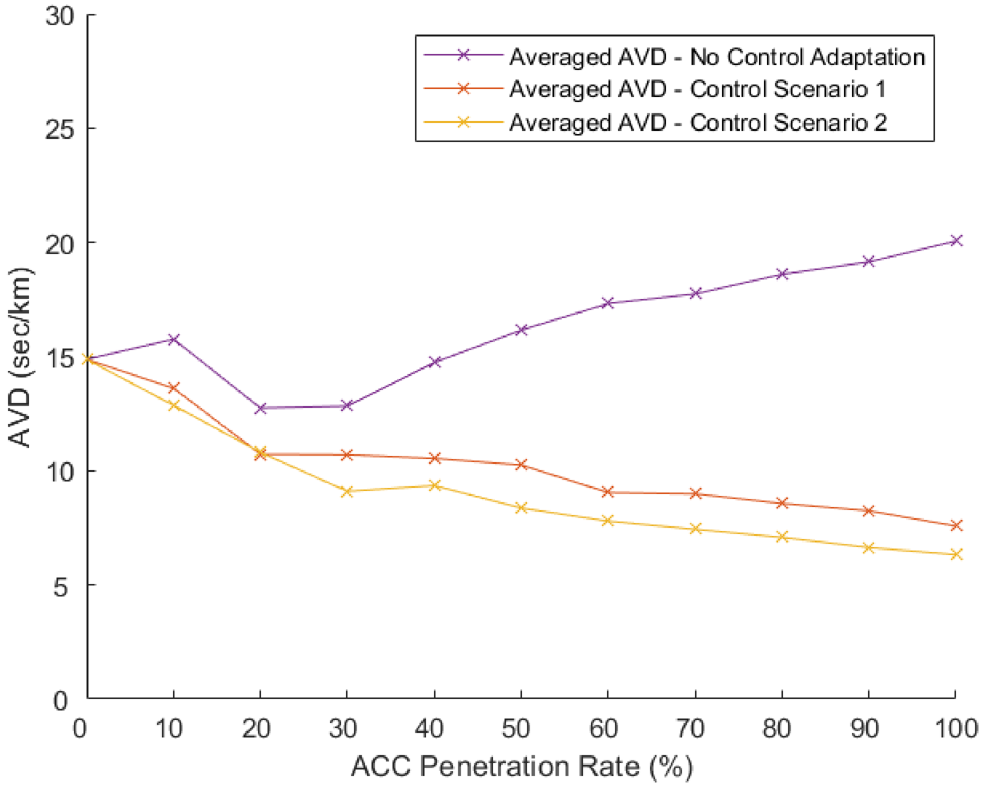

FIGURE 3.23: Comparison of the Average Vehicle Delay (AVD) for the No ACC Control Adaptation case, the ACC Control Adaptation scenarios 1 and 2 considering various PR

From Figures 3.24, 3.25, it is obvious that the difference between the ACC control adaptation scenario 1 and the no control adaptation case, and the difference between ACC control adaptation scenario 2 and no control adaptation case are steadily decreasing, while the difference between ACC control adaptation scenario 2 and ACC control adaptation scenario 1 remains somewhat constant. Table 3.4 also shows the somewhat constant percentage difference of scenario 2 versus scenario 1 in favour of scenario 2, with exact numbers.

	TTS($veh \times h$)			AVD($sec/veh/km$)		
PR	Control Case 1	Control Case 2	Difference(%)	Control Case 1	Control Case 2	Difference(%)
0%	-	-	-	-	-	-
10%	197.617	195.432	1.11	13.6122	12.863	5.5
20%	190.305	189.918	0.2	10.7216	10.8037	0.77
30%	190.431	185.501	2.59	10.6986	9.09563	14.98
40%	190.075	185.993	2.15	10.5452	9.34871	11.35
50%	189.272	183.301	3.15	10.252	8.36545	18.4
60%	185.378	181.475	2.11	9.04235	7.80668	13.67
70%	185.195	180.365	2.61	8.9868	7.43225	17.3
80%	183.922	179.308	2.51	8.56363	7.08006	17.32
90%	183.002	177.867	2.81	8.24538	6.63859	19.49
100%	180.854	176.915	2.18	7.57313	6.32809	16.44

TABLE 3.4: Difference between ACC Control Adaptation scenario 1 and 2 in Total Time Spent (TTS) and Average Vehicle Delay (AVD) metrics considering various PR

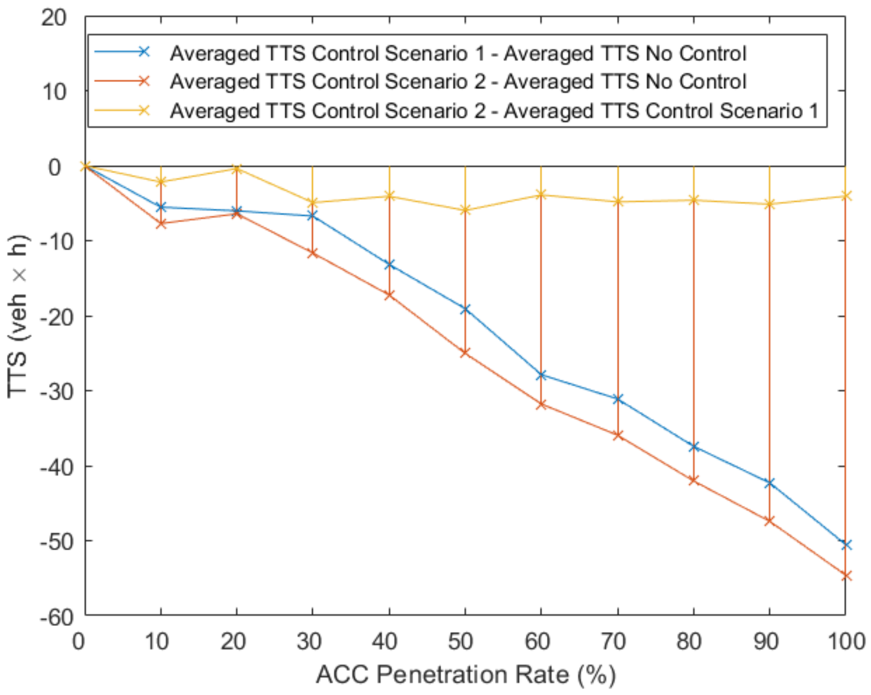

FIGURE 3.24: Subtraction of the Total Time Spent (TTS) between the No ACC Control Adaptation case, the ACC Control Adaptation scenarios 1 and 2 considering various PR

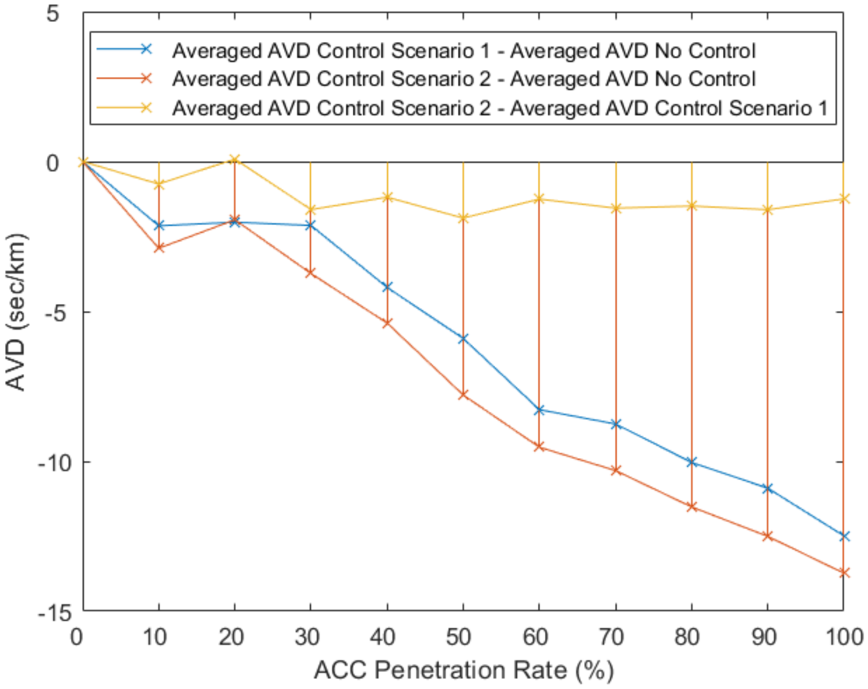

FIGURE 3.25: Subtraction of the Average Vehicle Delay (AVD) between the No ACC Control Adaptation case, the ACC Control Adaptation scenarios 1 and 2 considering various PR

CHAPTER 4

CONCLUSIONS AND FUTURE WORK

4.1 CONCLUSIONS

The objectives of this thesis were two. The first goal was the real-time collection and processing of real data from an existing network, and then, the successful estimation of traffic density in that network using an already developed Kalman filter. For this, the filter parameters have been appropriately tuned. Ideally, the speed measurements should be taken from CAVs via V2I communication, but since CAVs were not yet available, speed spot-sensors played the role of measuring speed. This means that the CAV-penetration rate can be considered 100%. In the end, the comparison between the estimation and the ground truth results clearly highlights the effectiveness of the Kalman filter used.

The second goal of the current thesis was the effective traffic control with CAVs, with the prerequisite of them having the ACC-ability in order to reduce, delay, avoid or even annihilate traffic congestion in a traffic simulation in the Aimsun Next tool, using the Gipps car-following model. In the control scheme, the control strategy based on the traffic flow and speed conditions suggested different time-gaps, with respect to which ACC control adaptation scenario it ran with. The first control adaptation scenario made an impact in reducing the congestion from small penetration rates, while the second control adaptation scenario was practically every time better than the first and it ended annihilating the congestion in high penetration rates. Contributing to the research, it was discovered that with the appropriate Sensitivity Factor per segment, the Gipps car-following model is able create a relatively severe congestion. For this, the increase of the Sensitivity Factor in merging areas and in areas with lane drops (active bottlenecks), and then, the gradual reduction for the segments after it, given the fact that these segments do not contain another active bottleneck, is proven determinant.

Concluding, in the real world there cannot and should not be flow detectors at every some hundred meters on a highway, as it would be very costly and would demand personnel all around the world for maintenance and part replacement. Therefore, the Kalman filter in the second chapter can be utilized in order for the control strategy in the third chapter to be applied and really prevent or even annihilate the formation of congestions in innumerable streets worldwide. So, traffic state estimation and traffic control by utilizing

VACS can improve the everyday life of people and the environment. Adopting these two ideas combined can revolutionize everyday transportation.

4.2 FUTURE WORK

In the near future, when the conditions for the road infrastructure permit, the infrastructure will be prepared to transceive vehicle-data via V2I communication, and then, research on traffic density estimation using real traffic data over various CAV penetration rates can be done.

On the other hand, it would be useful to try to employ the ACC control adaptation strategy on roads which surround a busy, commercial harbor like Antwerp's, where on a daily basis, at peak hours, there is active bottleneck congestion formed mostly by trucks. This is interesting, because trucks have much bigger size and weight, so their speeds, accelerations and movements, in general, are significantly slower. So, their time-gaps may differ, according to their size and load, and of course, there would also be other vehicle types of different speeds, sizes and time-gaps. Consequently, a network like this would be much more demanding, but finding a solution there would speed up the transportation of goods around the world, reduce emissions and save a huge amount of time, money and nerves that are unnecessarily being spent every day.

BIBLIOGRAPHY

[1] Markos Fountoulakis et al. "Highway traffic state estimation with mixed connected and conventional vehicles: Microscopic simulation-based testing". In: *Transportation Research Part C: Emerging Technologies* 78 (2017), pp. 13–33.

[2] S. Turksma. "The various uses of floating car data". In: *Tenth International Conference on Road Transport Information and Control, 2000. (Conf. Publ. No. 472)*. 2000, pp. 51–55. DOI: `10.1049/cp:20000103`.

[3] Wikipedia contributors. *Adaptive Cruise Control*. 2023. URL: `https://en.wikipedia.org/w/index.php?title=Adaptive_cruise_control&oldid=1163278736`.

[4] Nikolaos Bekiaris-Liberis, Claudio Roncoli, and Markos Papageorgiou. "Highway traffic state estimation with mixed connected and conventional vehicles". In: *IEEE Transactions on Intelligent Transportation Systems* 17.12 (2016), pp. 3484–3497.

[5] Diamantis Manolis et al. "Real time adaptive cruise control strategy for motorways". In: *Transportation research part C: emerging technologies* 115 (2020), p. 102617.

[6] Aimsun. *Aimsun Next 22 User's Manual*. Aimsun Next 22.0.1. Barcelona, Spain, 2022. [Online]. URL: `https://docs.aimsun.com/next/22.0.1/`.

[7] Peter G Gipps. "A behavioural car-following model for computer simulation". In: *Transportation research part B: methodological* 15.2 (1981), pp. 105–111.

[8] Vasileios Markantonakis et al. "Traffic control algorithms for mixed vehicle traffic–A simulation-based investigation". In: *Transportation Research Procedia* 52 (2021), pp. 356–363.

[9] Peter G Gipps. "A model for the structure of lane-changing decisions". In: *Transportation Research Part B: Methodological* 20.5 (1986), pp. 403–414.

[10] Georgia Perraki. "Evaluation of a model predictive control strategy on a calibrated multilane microscopic model". In: *Master's thesis, School of Production Engineering and Management, Technical University of Crete* (2016).

[11] Kai Yuan et al. “Capacity drop: a comparison between stop-and-go wave and standing queue at lane-drop bottleneck”. In: *Transportmetrica B: transport dynamics* 5.2 (2017), pp. 145–158.

[12] Yibing Wang et al. “Capacity Drop at Freeway Ramp Merges with Its Replication in Macroscopic and Microscopic Traffic Simulations: A Tutorial Report”. In: *Sustainability* 15.3 (2023), p. 2050.

[13] ISO/TC 204 Intelligent transport systems. *ISO 15622 — Intelligent transport systems — Adaptive cruise control systems — Performance requirements and test procedures*. 2018. URL: `https://www.iso.org/standard/71515.html`.

[14] Ty Bardwell et al. *Transportation Engineering Online Lab Manual: Traffic Flow Theory, Theory & Concepts, Speed-Flow-Density Relationship*. Oregon State University, Portland State University, University of Idaho. 2003. URL: `https://www.webpages.uidaho.edu/niatt_labmanual/`.

[15] Jiao Wang, Ronghui Liu, and Frank Montgomery. “Car-following model for motorway traffic”. In: *Transportation research record* 1934.1 (2005), pp. 33–42.

[16] Jiao Wang. “A merging model for motorway traffic”. PhD thesis. University of Leeds, 2006.

[17] Biagio Ciuffo, Vincenzo Punzo, and Marcello Montanino. “Thirty years of Gipps’ car-following model: Applications, developments, and new features”. In: *Transportation research record* 2315.1 (2012), pp. 89–99.